DOI: https://doi.org/10.2138/am-2021-7861. http://www.minsocam.org/

Revision 2

Zircon geochronological and geochemical insights into pluton building and volcanic-hypabyssal-plutonic connections: Oki-Dōzen, Sea of Japan - a complex intraplate alkaline volcano

Word count: 13739

JANE H. SCARROW[1,2*], KATY J. CHAMBERLAIN[3], PILAR MONTERO[1], MATTHEW S.A. HORSTWOOD[4], JUN-ICHI KIMURA[5], YOSHIHIKO TAMURA[5], QING CHANG[5], JENNI BARCLAY[2]

[1]Department of Mineralogy and Petrology, University of Granada, Campus Fuentenueva, Granada 18002, Spain

[2]School of Environmental Sciences, University of East Anglia, Norwich, NR4 7TJ, UK

[3]Environmental Sustainability Research Centre, University of Derby, Derby, DE22 1GB, UK

[4]British Geological Survey, Keyworth, Nottingham, NG12 5GG, UK

[5]Japan Agency for Marine-Earth Science and Technology, 12-15, Natsushimacho, Yokosuka, Kanagawa 237-0061, Japan

ABSTRACT

The relationship between plutonic and volcanic components of magmatic plumbing systems continues to be a question of intense debate. The Oki-Dōzen Islands, Sea of Japan, preserve outcrops of temporally associated plutonic, hypabyssal and volcanic rocks. Post-intrusion uplift juxtaposed Miocene syenites in inferred faulted contact with volcanic trachytes that are cut by rhyolite hypabyssal dikes. This provides a window deep into timing and origins of magma storage architecture and dynamics. Zircon is ubiquitous in all samples; our aim is to determine what its age and composition can reveal about the plutonic-volcanic connection. Here we show magma source characteristics are recorded in zircon Hf isotopes; source composition and assimilation of heterogeneous hydrothermally altered crust in zircon O isotopes; and extensive fractional crystallization in zircon trace elements. Combined with new U-Th-Pb SHRIMP zircon ages, 6.4–5.7 Ma, compositional data show pluton formation was by protracted amalgamation of discrete magma pulses. The rhyolite dike preserves an evolved fraction segregated from these discrete magmas. Synchronous with plutonism was volcanic eruption of trachyte magma derived from the same source, which may have stalled at a relatively shallow depth prior to eruption. Stalling occurred at least above the amphibole stability zone because amphibole-compatible Sc and Ti were not depleted in the trachyte melt resulting in elevated values of these in volcanic compared to plutonic zircon. Identifying smaller episodic magma pulses in a larger magmatic complex places constraints on potential magma fluxes and eruptible volumes. High-flux, large volume, plume-related ocean island magmatic systems may have extensive vertically distributed multi-stage magmatic reservoirs and subduction-related systems transcrustal magma reservoirs. By contrast, Oki-Dōzen was a low-flux system with incremental pluton growth and small- to moderate-scale eruptions.

Keywords: U-Th-Pb dating, zircon trace elements, O isotopes, Hf isotopes, amphibole

INTRODUCTION

Unerupted magma preserved as plutonic and hypabyssal rocks may provide a window deep into plumbing system architecture and dynamics of related volcanic rocks (e.g., Lipman, 1984; Barth et al. 2012; Deering et al., 2016). Plutonic magmatism may accumulate over protracted periods of time whereas associated volcanic systems magma may assemble rapidly before eruption (e.g., Mills and Coleman 2013; Caricchi et al. 2014, Coleman et al., 2016). Related to this temporal association-disassociation is a key question regarding components of magmatic complexes, do plutons preserve i) the erupted magma counterpart stalled and solidified at depth (e.g., Miller et al., 2011; Metcalf, 2004; Keller et al., 2015; Lipman and Bachmann, 2015) or ii) the residue left behind by extraction of erupted liquids (e.g., Bachmann and Bergantz 2004; Eichelberger et al. 2006; Gelman et al., 2014; Glazner et al., 2015; Lundstrom and Glazner, 2016; Cashman et al. 2017). Irrespective of details of their petrogenetic relationship with volcanic deposits, plutonic bodies record physical properties and compositions of magmas that did not erupt, e.g., viscosities, temperatures, volatile contents, and crystal cargoes. These may be compared and contrasted with extrusive products. These considerations are important in assessing potential connections in temporally associated plutonic and volcanic rocks; rarely, though, are systems dissected to reveal such relationships.

The Oki-Dōzen Islands, Sea of Japan, preserve outcrops of temporally associated plutonic, hypabyssal and volcanic rocks (Fig. 1). Brenna et al. (2015) studied the petrogenesis of the magmatic complex mafic and felsic volcanic rocks and exposed syenite. They presented a new hypothesis for the volcanic-plutonic connection in an intraplate context: the volumetrically significant proportion of felsic deposits (Fig. 1, Tiba et al., 2000) reflected a low magmatic flux coupled with crustal plumbing system heterogeneity that filtered magmas and permitted fractionation. Specifically, thermal destabilization and eruption triggered by injection of mafic magma into shallow evolved syenite magma bodies was impeded by a central network of vertically separated crustal reservoirs. This prevented large explosive eruptions typical of differentiated volcanic systems. However, questions remain regarding magma system longevity, magmatic source and the plutonic-hypabyssal-volcanic link. Significantly, as yet, there has been no systematic combined study of Oki-Dōzen zircon geochronology and mineral compositions.

Accessory minerals may provide information about magmatic processes not necessarily evident from whole-rock or major mineral phases, e.g., recycling in magma reservoirs and magma mixing (cf., Watson et al., 2006; Chu et al., 2009; Storm et al., 2014; Yan et al., 2018; Yan et al., 2020). They thus provide insights into temporal and compositional similarities and differences in the magmatic system plutonic-hypabyssal-volcanic components. Small-scale, short-lived magma storage regions, i.e., limited volume magma pulses (cf., Pitcher, 1979; Glazner et al., 2004) will have isolated, distinct, compositions and little evidence for crystal recycling. If plutonic rocks are the products of such short-lived episodes, then they may be temporally and compositionally linked to associated volcanism (e.g., Deering et al. 2016). If, on the other hand, the plutonic rocks preserve larger-scale, longer-lived magma storage and crystal accumulation they may track temporal and compositional variations in magma source and evolution (e.g., Storm et al., 2014). The Oki-Dōzen rocks are particularly well suited to address the question of magma storage architecture and timing because the current structural level exposes a vertical cross-section of the system permitting sampling of: felsic volcanic deposits, trachyte; associated plutonic rocks, syenites; and hypabyssal rhyolite dikes. In addition, the Brenna et al. (2015) model provides a framework to consider new data on the distribution and properties of magma reservoirs.

To decipher the volcanic-hypabyssal-plutonic connection we combine petrography, mineral compositions, whole-rock geochemistry, and zircon U-Th-Pb ages and Hf- and O-isotopes and trace elements. These data place temporal constraints on physical, thermal and compositional changes at given points in the magmatic plumbing system evolution.

GEOLOGICAL BACKGROUND

Oki-Dōzen is a composite intraplate alkaline volcano in the southern Sea of Japan. It lies ~15 km south-west of Oki-Dōgo Island and ~300 km northwest of the active subduction trench (Fig. 1a). Magmatism occurred on the Honshu continental shelf from 7–5 Ma (Brenna et al., 2015 and references therein) long after formation of the Sea of Japan, 21–14 Ma (Otofuji, et al. 1985). The volcano comprises three islands Nishinoshima, Nakanoshima and Chiburijima. A central Miocene pyroclastic cone is composed of the Takuhiyama trachyte sequence of breccias and tuffaceous flow units (5.7–6.2 Ma, U-Th-Pb zircon, Brenna et al., 2015). This has been eroded to reveal the hypabyssal and plutonic roots of the volcano (Figs 1 and 2). These outcrops form part of the Oki Islands National Park and UNESCO Global Geopark and have been the focus of numerous geological studies (e.g., Naemura and Shimada, 1984; Morris, 1986; Tiba, 1986; Morris et al., 1990; Wada et al., 1990; Kaneko, 1991; Brenna et al., 2015). In the center of the islands the Ōyama syenite (6–6.3 Ma, U-Th-Pb zircon, Brenna et al., 2015) has a surface expression < 2 km^2 and crops out in sub-vertical contact with the pyroclastic cone that is cut by radial trachytic-rhyolitic dikes (Fig. 2b). Baked contacts are absent in the trachytes as are chilled margins in the syenites.

In compiling the regional geological map Tiba et al. (2000) concluded the initial phase of dispersed 'upper somma' trachyte formation occurred between 6.3–5.3 Ma with caldera formation prior to trachyte eruption at ~5.4 Ma (Morris et al., 1990; Wada et al., 1990). Brenna et al. (2015) presented zircon U-Th-Pb ages that were mostly within error of the Tiba et al. (2000) results and interpreted the volcano as a basaltic nest with a trachyte–syenite core that filtered primitive magma injections in a multi-stage plumbing system. Numerous mafic dikes cut outer flank 'somma' trachybasalt, trachyandesits and basalt lava flows that surround the trachytic cone and associated syenites (Fig. 1). Mafic dikes do not crop out in the central complex, despite this trace element and isotopic compositional similarities indicate all the rocks fractionated, with minor crustal assimilation, from a single mantle-derived parent magma (Brenna et al., 2015). However,

DOI: https://doi.org/10.2138/am-2021-7861. http://www.minsocam.org/

geochronological and compositional complexities indicate the rocks do not represent a single undifferentiated magma. Syenite U-Th-Pb zircon ages span 1.4 My, 7.4–6.0 Ma, and whole-rock major and trace elements vary at each differentiation stage. This led Brenna et al. (2015) to invoke input from several distinct evolved magma batches into a shallow central reservoir (cf., Gudmundsson, 2012).

SAMPLING AND METHODOLOGY

Five representative samples of felsic volcanic, hypabyssal and plutonic Oki-Dōzen units were selected for detailed study (Fig. 1): one of dense lava from the Takuhiyama pyroclastic cone; three from geographically diverse areas of the Ōya a syenite; and one hypabyssal rhyolitic dike (Supplementary Material 1, Table 1). Studying the plutonic-volcanic connection using samples from juxtaposed plutonic and volcanic outcrops such as in the Oki-Dōzen Islands provides information about samples relative spatial distribution. For example, length scales of compositional and temporal variations may be assessed. Such information is lacking in studies of xenoliths in volcanic rocks. Samples were collected as large coherent blocks; any altered rind was removed in the field. Thin sections were made of all samples for petrographic examination, with remaining material prepared for geochemical analyses and mineral extraction. For full details of analytical methods and precision and accuracy see Supplementary Material 1.

One sample aliquot was retained and powdered for whole-rock X-Ray Fluorescence analysis of major and trace elements at the Japan Agency for Marine Earth Science and Technology (JAMSTEC). Major element analyses of mineral phases in polished thin sections were performed using wavelength dispersive spectroscopy on a JEOL JXA-8500F Electron Probe Micro-Analyser at JAMSTEC. In-situ major and trace element analyses of feldspar and amphibole were performed using Laser Ablation Inductively Coupled Plasma Mass Spectrometry (LA-ICPMS) at JAMSTEC. Zircon was analyzed for U-Th-Pb and oxygen isotopes using the IBERSIMS SHRIMP IIe/mc ion microprobe at the University of Granada Scientific

Facilities Center (CIC-UGR). Zircon trace element concentrations were analyzed at the CIC-UGR LA-ICPMS laboratory using a Perkin Elmer NexION 350X ICP-MS coupled to a New Wave Research NR 213 LA system. Laser ablation Hf isotopes were determined at the British Geological Survey, Keyworth, United Kingdom, on the same zircon as the O isotopes, using a ThermoScientific Neptune Plus MC-ICP-MS.

RESULTS

PETROGRAPHY

The trachyte sample (OD-1) is leucocratic, holocrystalline, with a fine-grained inequigranular porphyritic texture (Fig. 2g). Phenocrysts, 30 modal %, are predominantly euhedral alkali feldspar, up to 4 mm diameter, with minor plagioclase, quartz, clinopyroxene and Fe-Ti oxides (± amphibole, ± biotite microphenocrysts). The groundmass is patchy micro- to cryptocrystalline. Zircon and apatite are accessory minerals. The predominantly anhedral amphibole phenocrysts do not appear to be in equilibrium with the groundmass showing evidence of corrosion and reaction (Fig. 2g). Secondary minerals include chlorite and clays.

The rhyolite sample (OD-25) is leucocratic, holocrystalline, with a fine-grained inequigranular porphyritic texture (Fig. 2h). Phenocrysts, 30–40 modal %, are individual and glomerocrysts of euhedral-subhedral alkali feldspar, up to 7 mm diameter, minor quartz and Fe-Ti oxides in a microcrystalline groundmass. Zircon and apatite are accessory minerals. The alkali feldspar is weakly saussuritized.

Syenite samples (OD-4, OD-5 and OD-22) are leucocratic, holocrystalline, phaneritic medium-coarse grained rocks with inequigranular hypidiomorphic textures and variable development of a late-stage interstitial agpaitic-like mosaic of amphibole and myrmekitic quartz (Fig. 2i). The mineral assemblage consists of 5–10 mm diameter euhedral alkali feldspar with microperthitic exsolutions (80–85 modal %), and minor subhedral amphibole, clinopyroxene, biotite, Fe-Ti oxides and quartz. Zircon and rare, albeit relatively large (<0.5 mm), apatite are accessory minerals (as well as La- and Ce-rich phase chevkinite, Brenna et al. 2015). Secondary minerals include clays.

MAJOR MINERAL COMPOSITIONS

Feldspars in the syenites are Ca-poor, with compositions of sanidine to anorthoclase (Ab_8Or_{92} to $An_{10}Ab_{58}Or_{32}$; see Supplementary Material 2 for the full dataset and ternary diagram). None of the samples show evidence for core–rim compositional zoning and no zoning is observed within the BSE images. The trachyte sample feldspar compositions vary between sanidine ($An_2Ab_{48}Or_{50}$) and andesine ($An_{44}Ab_{51}Or_5$), with no compositional differences between core and rim (see Supplementary Material 2). Feldspars from the rhyolite dike have relatively restricted compositions between $An_1Ab_{65}Or_{34}$ and $An_7Ab_{65}Or_{28}$, again, no differences were measured between crystal interior and rim zones.

Amphibole is the most prevalent mafic phase in all rock types, except the rhyolite, it has compositions of ferro-edenite or ferro-hornblende (nomenclature of Leake et al., 2003). No systematic differences in amphibole composition are observed between samples of syenite, or between syenite amphiboles and the minor trachyte amphibole. Trace element abundances are reported in Supplementary Material 2, Sc varies between 22 and 221 ppm in syenite amphiboles.

WHOLE-ROCK GEOCHEMISTRY

Whole-rock major and trace element data for the syenites, trachyte and rhyolite dike are given in Fig. 3 and Supplementary Material, Table 1. They have median values within published compositional ranges for each rock type (cf., Brenna et al., 2015 and references therein).

Whole-rock data have a point of inflection at 65 wt% SiO_2 that divides the syenites and trachyte from the rhyolite (Fig. 3). All the rocks have an alkaline metaluminous character (SiO_2 62–65 wt%; Na_2O+K_2O

10.4–12 wt%), except the rhyolite which is alkaline and weakly peraluminous (SiO_2 73 wt%; Na_2O+K_2O 10.3 wt%). The FeO_T/MgO has a wide range (5.73–17.82) and K_2O is elevated (5.4–6.4 wt%) (Fig. 3a and b, Supplementary Material 1, Table 1). Below 65 wt% SiO_2 the concentrations of MgO, FeO_T, CaO, TiO_2 and P_2O_5 as well as V, Sc and Sr, correlate negatively with SiO_2, at more evolved compositions the trends flatten. No clear trend is evident in Al_2O_3 below 65 wt% SiO_2, above this it correlates negatively with SiO_2 (Fig. 3c). The only major elements that correlate positively with SiO_2 are K_2O and Na_2O, increasing to 65 wt% SiO_2 then decreasing; Ba also follows this trend albeit more weakly. Only Sc shows a clear negative correlation with SiO_2 (Fig. 3e). Various trace elements, Zr, Y, Th, Pb, Nb, Rb and Ga show a broad positive correlation with SiO_2 (e.g., Fig, 3f); MnO, Cr and Ni do not correlate with SiO_2.

Normalized to N-MORB all the rocks have comparable profiles: positive anomalies in K, Pb, Zr and Y and negative anomalies in U, La, Sr and Ti. The rhyolite dike (OD-25) also has marked negative anomalies in Ba and Eu (Fig. 3g). In addition, normalized to chondrite, the rocks are enriched in light rare earth elements (LREE) relative to heavy rare earth elements (HREE). The least evolved, lowest SiO_2, syenite (OD-22) and the trachyte (OD-1) do not have negative Eu anomalies whereas the two more evolved, higher SiO_2, syenites (OD-4 and OD-5) have slight negative Eu anomalies; the evolved rhyolite dike (OD-25) is quite depleted in Eu (Fig. 3h). One of the more evolved syenites (OD-4) has a weak negative Ce anomaly, the other syenites and the trachyte no Ce anomaly and the rhyolite dike a weak positive Ce anomaly (Fig. 3h).

ZIRCON U-Th-Pb SHRIMP GEOCHRONOLOGY

The U-Th-Pb SHRIMP data are presented in Fig. 4 and Supplementary Material 1, Table 2. Representative cathodoluminescence (CL) zircon images from the 5 studied samples are included in Supplementary Material 3. No textural evidence was detected for more than one stage of zircon growth, e.g., inherited cores, resorption surfaces or overgrowth rims. However, in some zircon grains subsolidus hydrothermal alteration was detected as murky or fluid inclusion-rich pitted textures - these regions were avoided during analysis. The majority of zircon analyzed from the five samples had a small, but measurable, amount of common-lead. This may be significant when considering low concentration of radiogenic lead generated in young (<7 Ma) zircon. Of available common-lead correction methods the one based on ^{207}Pb is usually best for young zircon (Tera and Wasserburg, 1972) and was used here. We also checked our results using the 208-based correction method (Faure, 1986) which, in general, gave good results, yielding ^{206}Pb/^{238}U dates close to concordia and 207-corrected dates, but usually with larger errors and MSWDs caused by error propagation.

We selected 22 representative zircon grains from trachyte OD-1 for U-Th-Pb analysis. Centers and edges of morphologically different, higher to lower CL zircon were analyzed. Nevertheless, all data points align in a Wetherill concordia on a well-defined common lead discordia line yielding a lower intersection date of 5.94 ± 0.20 Ma (Fig. 4a). Individual date errors are quoted at 1σ, mean dates at 2σ. The 207-corrected dates yield a weighted-mean ^{206}Pb/^{238}U date of 5.89 ± 0.16 Ma, MSWD=1.08, within-error of the lower intercept date.

From rhyolite OD-25 we analyzed 25 points on 24 zircon grains, 20 of them in the darker CL centers or intermediate parts of the crystals and 5 in the lighter CL edges. In both cases we selected unzoned and oscillatory-zoned areas. Two analyses were rejected because of poor quality, high error (± ~3 My, not included). Of the rest, 19 plot in a Wetherill concordia diagram along a common-lead discordia line yielding a lower intersection date of 5.58 ± 0.15 Ma and a 207-corrected weighted-mean ^{206}Pb/^{238}U date of 5.65 ± 0.12 Ma, MSWD=2.0. Both dates are identical within-error (Fig. 4b). Despite the CL morphological differences, the crystals centers and edges are the same age. Four remaining points are slightly older even though they are morphologically indistinguishable from the others. They plot along a different common lead discordia, parallel to but above the main one (Fig. 4b). These 4 points yield a lower intersection date of 6.75 +0.34/-0.47 Ma and a 207-corrected weighted-mean ^{206}Pb/^{238}U date of 6.75 ± 0.16 Ma, MSWD =0.40.

Twenty-two U-Th-Pb analyses were performed on 22 zircon from syenite OD-4. Most analyses were done on clean, transparent, pinkish, zoned-unzoned moderate-intensity CL crystals. Five analyses were done on the white opaque crystals partially affected by fluids, murky or fluid inclusion-rich pitted texture, but in areas free from inclusions. Two of these 5 analyses, plus another two from the main population, were rejected because they had large errors (± 0.98 My and ± 2.38 My, analyses not included). In a Wetherill concordia diagram the remaining 18 analyses plot on a well-defined common lead discordia with two data points being concordant. They yield a lower intersection date of 6.13 +0.14/- 0.26 Ma and a 207-corrected weighted-mean $^{206}Pb/^{238}U$ date of 6.38 ± 0.10 Ma, MSWD = 0.65 (Fig. 4e), both dates are within error.

We selected 18 zircon grains for U-Th-Pb analyses from syenite OD-5 including centers and edges, low to high CL intensity and unzoned to variably zoned crystals. All 18 analyzes are discordant and align in a Wetherill concordia diagram on a common-lead discordia yielding a lower intersection date of 6.21 +0.18/- 0.24 Ma (Fig. 4d). The 207-corrected dates give a weighted-mean $^{206}Pb/^{238}U$ date of 6.10 ± 0.08 Ma, MSWD 1.23 (Fig. 4d), both dates are within-error.

Twenty zircon including centers and edges of high to low CL and oscillatory zoned to unzoned crystals were selected for U-Th-Pb analysis from syenite OD-22. In a Wetherill concordia diagram all plot on a common lead discordia line yielding a lower intersection date of 5.60 ± 0.21 Ma. The 207-corrected weighted-mean $^{206}Pb/^{238}U$ date is 5.72 ± 0.11 Ma, MSWD =1.1 (Fig. 4c), both dates are within-error of each other. The dates are 0.3–0.4 My younger than published ages, but within uncertainty (Brenna et al., 2015).

From our data, two groups of zircon dates may be identified: the first comprising volcanic (OD-1), hypabyssal (OD-25) and one plutonic sample (OD-22). The samples mean dates form a group that are not significantly different from each other. The other two plutonic samples (OD-4 and OD-5) means are, however, significantly older than the first group.

ZIRCON COMPOSITION

Zircon trace element and O isotopes data are presented in Figs 5–8 and, with Hf isotopes, in Supplementary Material 3 along with the background rationale for zircon compositional data interpretation. Despite similarity of plutonic syenites and volcanic trachyte whole-rock compositions (Fig. 3, Supplementary Material 1, Table 1) there are differences in their zircon trace element and isotopic compositions. These record hand specimen scale heterogeneity over a limited time, preserving a snapshot of magma crystallization history (Figs 5–8). The more evolved hypabyssal rhyolite has different whole-rock and distinctive zircon compositions. No correlation was observed between zircon age and any trace element concentration or ratio.

TRACE ELEMENTS. The Oki-Dōzen zircon REE concentrations vary considerably (Figs 5 and 6 and Supplementary Material 3) consistent with typical intra-grain and inter-grain compositional variations in other magmatic zircon (cf., Hoskin and Schaltegger, 2003). Zircon affected by post-crystallization hydrothermal alteration have murky or fluid inclusion-rich pitted textures (cf., Hoskin, 2005; Jiang et al., 2019) and/or flat chondrite-normalized LREE patterns and small Ce anomalies (Hoskin, 2005; Zhong et al. 2018). Zircon that contains tiny inclusions of LREE-rich minerals (e.g., allanite, chevkinite) or fluid inclusions also have elevated La values atypical of magmatic zircon (Hoskin and Schaltegger, 2003; Claiborne et al., 2010; Ni et al., 2020). Oki-Dōzen zircon with these textural or compositional features were removed from the data set leaving only unaltered primary magmatic grains.

Within single rock samples zircon LREE concentrations vary by up to two orders of magnitude and HREE concentrations by an order of magnitude (Fig. 6 and Supplementary Material 3). The range is greatest in the oldest syenite, OD-4, but comparable in the other samples. All plutonic, hypabyssal and volcanic zircon chondrite-normalized REE patterns are parallel-subparallel and have similar, typically magmatic, depletion in

LREE relative to HREE ($[Gd/Yb]_N$ 0.03–0.16) and positive Ce and negative Eu anomalies relative to adjacent REE (cf., Hoskin and Schaltegger, 2003).

In the dataset as a whole the zircon Eu anomalies are moderately to strongly negative, Eu/Eu* (0.003–0.186) indicative of feldspar fractionation under reducing conditions, with one value of 0.35 (Eu = Eu_N and Eu* = $[Sm\times Gd]_N^{0.5}$) (Fig. 6, Supplementary Material 3). These are akin to dike whole-rock value but differ from volcanic and plutonic whole-rock data that have weakly negative to positive Eu anomalies (Fig. 3). More specifically, zircon from the plutonic rocks have smaller and more consistent Eu/Eu* (0.024–0.140) than those from the hypabyssal rocks that are generally lower (0.005–0.06) or the volcanic rocks that are generally higher (0.003–0.350). Prominent negative Eu/Eu* ratios seen in all the Oki-Dōzen zircon do not correlate systematically with Zr/Hf, a magma differentiation index that reflects melt Zr depletion relative to Hf as zircon fractionates (Claiborne et al., 2006a). The plutonic and hypabyssal zircon Eu anomalies are relatively constant. The volcanic trachyte zircon has variable Eu anomalies at a given differentiation level.

The zircon Ce anomalies are positive, Ce/Ce* (2.95–51.56, where Ce = Ce_N and Ce* = $[La\times Pr]_N^{0.5}$) indicative of oxidizing conditions in the magmatic system. Whole-rock Ce anomalies, by contrast, are only weakly positive to negative (Fig. 3h). Zircon from the plutonic rocks have larger and more variable Ce/Ce* (6.90–51.56) than those from the hypabyssal (4.02–26.03) and volcanic rocks (2.95–11.74) (Fig. 6).

Other zircon trace element concentrations are also heterogeneous e.g., Hf (~5,000–18,500 ppm) and U (23–1202 ppm, with 3 values up to ~12,700 ppm in the syenite OD-4). Also, U/Yb varies (0.7 ± 0.26) within the range 0.2–4 of typical igneous zircon (Hoskin and Schaltegger, 2003). The Th/U ratios (1.2 ± 0.7, with 2 values up to ~3.8 in the syenite OD-4) are also typical of igneous values ≥0.5.

The plutonic syenite zircon have the broadest Zr/Hf range from (38–100: OD-4 ~55–100; OD-5 ~40–90; OD-22 ~50–70) (Fig. 5). The volcanic trachyte zircon have a spread of Zr/Hf from 43–81 and the hypabyssal rhyolite zircon the narrowest of 61–80. Few elements show clear correlations with the Zr/Hf differentiation index, but compositional differences between samples and covariances in individual samples are apparent, e.g., in syenite OD-5. Although overlap exists, a division may be made between the volcanic and hypabyssal rocks and plutonic rocks zircon compositions: OD-4 syenite zircon generally have lower concentrations of elements that are compatible in zircon, e.g., Ti and Sc; zircon from the syenite OD-5 has higher values of these elements; and syenite OD-22 and most notably OD-1 trachyte zircon the highest values (Fig. 5). The rhyolite OD-25, on the other hand, has variable concentrations of zircon-compatible elements (Fig. 5). All three plutonic samples show typical trace element fractionation trends: Ti correlates positively with Zr/Hf (Fig. 5a); as does Th/U and $(Gd/Yb)_N$; whereas U and U/Yb correlate negatively (Fig. 5). In contrast to the syenites, Ti does not correlate with differentiation in the trachyte nor the rhyolite (Fig. 5a).

In the Grimes et al. (2015) tectonomagmatic discrimination diagram (Fig. 7) all the Oki-Dōzen zircon plot in the high U/Yb, continental crust input or enriched mantle source fields.

O AND HF ISOTOPES. The Oki-Dōzen zircon O isotope data are heterogeneous, $\delta^{18}O$ is reported relative to VSMOW. Values range from well below typical of mantle (4.7–5.9 ‰) to higher typical of continental crust (> 6 ‰) (Fig. 8) (cf., Valley, 2003). The oldest syenite, OD-4, $\delta^{18}O$ range is 5.23–6.78 ± 0.08 ‰ (2σ). Syenite OD-5 has the broadest $\delta^{18}O$ range (3.24–7.94 ± 0.07 ‰) whereas the youngest syenite, OD-22, has low $\delta^{18}O$ (2.89–4.69 ± 0.09 ‰) comparable to the volcanic trachyte, OD-1, $\delta^{18}O$ (3.62–5.64 ± 0.08 ‰). All the hypabyssal rhyolite dike, OD-25, zircon compositions fall below the mantle range, $\delta^{18}O$ (2.89–4.69 ± 0.07 ‰). The $\delta^{18}O$ values do not correlate with differentiation (Zr/Hf) nor age.

Zircon Hf isotope ratios are sensitive to magma composition variations which may reflect source compositions. Depleted mantle has high εHf_t, >15, more enriched sources, e.g., continental crust, have lower values, <0 (Hawkesworth et al., 2010). The Oki-Dōzen zircon Hf isotope data are more uniform than the O isotope data; sample means are all the same within 2σ error (see Supplementary Material 3). The older syenite OD-5 εHf_t mean is -3.65 ± 0.65 (n=13); the younger syenite OD-22 has a mean of -3.80 ± 0.48 (n=16). The hypabyssal rhyolite dike, OD-25, mean is -3.66 ± 0.45 (n=15), changing to -3.98 ± 0.63 (n=13) when the two highest values are excluded. The volcanic trachyte, εHf_t mean = -3.84 ± 0.63 (n=13). All means are within error. The εHf_t values do not correlate with $\delta^{18}O$, differentiation (Zr/Hf), age nor Ti.

INTENSIVE VARIABLES

Major element concentrations in mineral phases and whole-rock XRF analyses, taken as a proxy for melt compositions, have been used to apply various thermobarometric models for the magmatic condition of mineral formation. Variables modeled using different thermobarometers applied to the same samples are compared with the results of Brenna et al. (2015). They calculated higher temperature and pressure stalling for the trachyte and shallower, cooler stalling for the syenite (Fig. 9; Brenna et al., 2015).

Feldspar-melt thermometry was applied to all samples where chemical equilibrium between feldspar and host rock could be demonstrated (following Putirka, 2008) and following petrographic assessment of feldspar textures (see Petrography section). The trachyte has temperatures between 950–970 °C, whereas two of the syenites have a broader range of temperatures that overlap with the trachyte: 880–1020 °C. The third syenite sample, OD-22, has higher, 1020 °C, temperatures reflected in plagioclase-melt compositions, but also has anomalously low temperatures from alkali feldspar-melt compositions, ~690 °C (Fig. 9). The rhyolite dike yields significantly lower alkali feldspar-melt temperatures between 700 and 760 °C.

Amphibole-melt thermometry (Molina et al., 2015) and amphibole thermobarometry (Ridolfi and Renzulli, 2012) have been applied to the syenite samples. No equilibrium amphibole was found in the rhyolite dike nor trachyte, so estimates were not obtained. Although the Ridolfi and Renzulli (2012) calibration assumes a 13-cation composition of amphiboles (after Leake et al., 1997) both thermometers are comparable. The Molina

This is the peer-reviewed, final accepted version for American Mineralogist, published by the Mineralogical Society of America.
The published version is subject to change. Cite as Authors (Year) Title. American Mineralogist, in press.
DOI: https://doi.org/10.2138/am-2021-7861. http://www.minsocam.org/

et al. (2015) calibration yields slightly higher temperatures (Fig. 9) than the Ridolfi and Renzulli (2012) calibration. From this latter calibration syenite temperatures are 855–1010 °C.

Ti-in-zircon thermometry (Watson and Harrison 1983; Ferry and Watson, 2007) using zircon LA-ICPMS analyses was undertaken assuming an $a\mathrm{SiO_2}$ of 1 given the presence of quartz (see Petrography section). Co-existing oxides are not present and therefore limit a robust estimation of activity of Ti (cf., Ghiorso and Gualda, 2013). We have assumed a range of activities for $a\mathrm{TiO_2}$ between 0.2 and 0.7. Lower values of $a\mathrm{TiO_2}$ produce Ti-in-zircon temperatures that are better aligned with other thermometric techniques. More significant than absolute values of temperatures, however, are comparisons between modeled temperatures, at $a\mathrm{TiO_2} = 0.2$: syenites, 763–1007 °C; the trachyte, 839–1181 ºC, and the hypabyssal rhyolite dike, 811–950 °C. High temperatures for the evolved dike zircon suggest they are antecrysts, unlike the large alkali feldspars rims that record final growth at lower temperatures than the syenite (Fig. 9).

Pressure estimates are limited by available phases. Whereas composition of amphibole has been suggested to be directly related to pressure of crystallization many uncertainties exist, with large variations in modeled pressures depending on how cation distributions are calculated (cf., Humphreys et al., 2019). Using amphibole compositions from both the present study and Brenna et al (2015) calculations with the Ridolfi et al. (2010) cation calculator and the calibration of Ridolfi and Renzulli (2012) gives pressures of 190–620 MPa for the syenite. This range overlaps with and extends to greater depth the cpx-melt pressure estimates for the trachyte, 210–390 MPa, of Brenna et al. (2015) who used the Masotta et al. (2013) calibration.

THE PLUTONIC-HYPABYSSAL-VOLCANIC CONNECTION

THERMOBAROMETRY - PHYSICAL CONDITIONS OF MAGMATISM

Alkaline magmatic systems present challenges for constraining intensive variables because of their silica-undersaturated nature and the limited number of thermobarometers which are calibrated for such systems. By

DOI: https://doi.org/10.2138/am-2021-7861. http://www.minsocam.org/

applying multiple thermometers to the plutonic, volcanic and hypabyssal samples we tested the consistency of the different systems. This placed further constraints on the nature of the system that fed the silicic magmatism of Oki-Dōzen from ~7–5 Ma.

Comparison of feldspar-melt temperature estimates (Putirka, 2008) with amphibole-melt temperatures (Ridolfi and Renzulli, 2012; Molina et al., 2015) yielded very similar values for each sample (Fig. 9). Small differences between thermometers in individual samples are not consistent with, but are largely contained within, the range of modeled values if an uncertainty of ± 20 °C is assumed (Fig. 9). Alkali feldspar-melt temperatures from the syenite OD-22 are the only significantly lower major phase temperature estimates, potentially from late-stage feldspar hydrothermal alteration as previously noted by Brenna et al. (2015).

In contrast to major phase thermometry, application of the Ti-in-zircon thermometer (Ferry and Watson, 2007) yields large ranges in modeled temperatures in individual samples e.g., up to 340 °C at $a\mathrm{TiO_2} = 0.2$ in the trachyte sample. In addition, temperatures are systematically lower than major phase thermometers (Fig. 9). Other studies have noted significantly lower Ti-in-zircon temperatures when compared with major phases (e.g., Chamberlain et al., 2014, Schiller and Finger, 2019). The difference may be the result of zircon crystals not representing the same magmatic stage as major phases; however, the presence of zircon as inclusions within major phases makes this unlikely. So, incorrect assumptions made when applying the Ti-in-zircon thermometer probably account for differences in Ti-in-zircon temperatures and major phase thermometry. Given the absence of rutile in Oki-Dōzen samples $a\mathrm{TiO_2}$ must be < 1 and for Ti-in-zircon temperatures to align with major phase thermometry $a\mathrm{TiO_2}$ of < 0.2 are required. This is significantly lower than has been suggested for many volcanic systems (cf., Hayden and Watson, 2007; Reid et al., 2011; Ghiorso and Gualda, 2013). Even so, recent studies have highlighted $a\mathrm{TiO_2}$ (and to a lesser degree, aSiO2) may evolve throughout crystallization of plutonic bodies (Schiller and Finger, 2019). This implies assumption of a uniform $a\mathrm{TiO_2}$ may not be valid, especially for plutonic rocks. The large ranges in Ti-in-zircon temperatures (Fig. 9) reflects the range in Ti concentrations (4–20 ppm) within individual samples. Irrespective of their volcanic, plutonic or hypabyssal origin this may reflect: a non-uniform $a\mathrm{TiO_2}$; the presence of nanoscale inclusions where Ti is not a structural component (cf., Chamberlain et al., 2014); or a combination of these factors. It is clear Ti-in-zircon thermometry lacks constraints to place absolute values on magmatic temperatures. However, it is useful here for comparing 'relative' differences between the volcanic, hypabyssal and plutonic samples from the same magmatic system - where $a\mathrm{TiO_2}$ and $a\mathrm{SiO_2}$ are likely to have been similar.

Application of multiple thermometers has highlighted clear differences between the volcanic, plutonic and hypabyssal samples. Major phase thermometry shows consistent average temperatures for the trachyte and syenite at ~930 °C. This is in contrast to the ~50 °C difference suggested by Brenna et al. (2015) who applied different thermometers to the volcanic and plutonic samples. Whereas average temperatures are consistent between volcanic and plutonic samples the range in major-phase-modeled temperatures is larger for the syenite samples than the trachyte. This is consistent with a more protracted period of melt evolution in the plutonic bodies. The hypabyssal rhyolite dike has Ti-in-zircon ranges that are well-aligned with syenite values and ranges. By contrast, a significantly lower alkali feldspar-melt modeled temperature is potentially the result of late-stage alteration in a hydrothermal system, as also seen in the syenite OD-22. Therefore, these lower ~700 °C temperatures are not interpreted to reflect true magmatic conditions.

Application of barometric techniques is limited by available mineral phases and lack of a well-calibrated barometer for these ferro-edenite amphiboles (Humphreys et al., 2019). Nevertheless, it would appear that similar to thermometric estimates the syenites also record comparable pressures to the trachyte, but with a larger range. We interpret this as the result of amphibole crystallization over an extended range of depths within the crust. An alternative would be temperature-controlled chemical exchanges (cf., Shane & Smith, 2013) producing a range of apparent pressures due to variable $^{VI}\mathrm{Al}$ (e.g., Thornber et al., 2008). The range in crystallization pressures could be explained by: mixing of mafic and felsic magmas (e.g., Scarrow et al, 2009); or, accumulation of xenocrystic material during ascent (e.g., Ridolfi et al., 2010). That said, compositional and textural observations are inconsistent with a mixed or xenocrystic origin because amphiboles: lack zoning or reaction rims in the syenites; and, are present as later-stage, e.g., interstitial subhedral mineral phases. So, syenite body formation through accumulation of multiple polybaric melts is our preferred explanation for the variation in intensive variables (cf., Michel et al., 2008; Farina et al., 2012).

GEOCHRONOLOGY - DURATION OF MAGMATISM

Precise U-Th-Pb zircon ages presented here show the studied magmatism lasted for at least ~1 My from ~5.5–6.5 Ma (Fig. 4). This is within the ~2 My range of published K-Ar and zircon U-Th-Pb ages for the syenite (7.5–5.6 Ma) and ~1 My range for the trachyte (6.0–5.4 Ma) and dikes (6.0–5.5 Ma) (Morris et al., 1997; Tiba et al., 2000; Brenna et al., 2015**)** (Fig. 4). Our new zircon age and trace element data highlight at least two separate magma pulses coalesced to form the syenite body. We can divide the magmatism into two main groups with mean zircon U-Th-Pb dates that are significantly different from each other (95% confidence level). The older group comprises two syenites, OD-4: 6.38 ± 0.10 Ma and OD-5: 6.10 ± 0.08 Ma; the younger group is composed of syenite, OD-22: 5.72 ± 0.11 Ma, the volcanic trachyte, OD-1: 5.89 ± 0.16 Ma, and the coeval hypabyssal rhyolite dike, OD25: 5.65 ± 0.12 Ma (Fig. 4). Plutonism duration is consistent with previous studies of intrusive rocks in intraplate settings (e.g., Allibon, et al., 2011) and identification of the role of multiple magma batches in forming plutons (e.g., Glazner et al., 2004). Our new data temporally link the plutonic, hypabyssal and volcanic components of the system (Fig. 4).. Furthermore, five older, antecrystic, grains detected in the hypabyssal and volcanic rocks (6.7–7.2 Ma) indicate en route to the surface the magma traversed, and scavenged, zircon from the remains of older magmatic events. This extends the duration of magmatism to > 2 My. Consistent with this is the more heterogeneous bimodal spread of zircon dates in the hypabyssal and volcanic rocks, which contrasts with the unimodal peak in the three plutonic samples (Fig. 4).

Brenna et al. (2015) proposed two potential end member models for the Oki-Dōzen magmatism: either, both intrusive and extrusive rocks were formed by single discrete events with the syenite, 6.2 Ma, crystallizing before the trachyte, 5.9 Ma; or, from the zircon ages and U composition in the two rock types, both volcanic and plutonic activity was more prolonged and pulsatory with plutonism lasting ~1 My and trachyte magmatism lasting ~0.5 My. Our new zircon ages are consistent with the second model. To further differentiate between models, age data can be linked to variations in zircon trace element compositions.

ZIRCON COMPOSITION

MAGMA SOURCE. Isotopic and trace element compositions of zircon may be used to infer magma source (e.g., van de Flierdt et al., 2007, Grimes et al., 2015). The continental crust intraplate context of the Oki-Dōzen Islands west of the active subduction trench in the southern Sea of Japan is reflected in key zircon trace elements tectonomagmatic discrimination diagrams (Fig. 7) (Grimes et al., 2015). None of the Oki-Dōzen samples have typical MOR low U/Yb ratios, <0.1 (cf., Grimes et al., 2015) (Fig. 7a). In the Sc/Yb versus Nb/Yb diagram they plot in the continental field (Fig. 7b); in the 'crustal input or enriched mantle source' in the U/Yb versus Hf diagram (Fig. 7c); and, in the amphibole-rich region of the Ti versus Sc/Yb plot (Fig. 7d). It appears diagrams that include Sc best discriminate continental and arc character whereas Nb highlights plume influence, i.e., mantle source enrichment relative to MORB. In contrast to the predominantly Mesozoic datasets used in constructing the tectonomagmatic discrimination diagrams our zircon are younger, Cenozoic–Late Miocene.

Significantly, the trace element data do not show clear differences in source between the plutonic, hypabyssal and volcanic samples. This is consistent with mean Hf isotope values that vary from -3.65 ± 0.65 and -3.80 ±

0.48 for the syenites, -3.66 ± 0.75 for the rhyolite dike, to -3.84 ± 0.63 for the volcanic trachyte. Notably, εHf_t means of the two analyzed syenites OD-5 and OD-22 plus the trachyte OD-1 all have an MSWD value close to 1 indicating these data represent single populations. The rhyolite dike εHf_t mean, by contrast, has an MSWD of 2.1, greater than would be expected for a single population. Nevertheless, the similarity of the means suggests derivation from the same source. Negative εHf_t values are typical of continental rocks (e.g., van de Flierdt et al., 2007) consistent with assimilation of a continental crust component indicated by the zircon trace elements (Fig. 7). Typical whole-rock εHf_t values for Quaternary volcanic rocks from the nearby Ulleung and Dok islands are also ~ -3 (Choi et al., 2013). The new zircon Hf isotope and trace element data suggest the evolved magmatic rocks of the central Oki-Dōzen complex are products of a similar degree of partial melting of a vertically and laterally restricted region of upper mantle. This inference is in agreement with the work of Brenna et al. (2015) who compared whole-rock major and trace element and Sr and Nd isotope data from the Oki-Dōzen central and flank primitive alkaline ocean island (OIB)-like basalts.

In contrast to trace element and Hf isotopic data, the Oki-Dōzen zircon $\delta^{18}O$ values are quite variable (2.89–7.94 ‰) from well-below to well-above typical mantle values of 5.3 ± 0.3 ‰ (Fig. 8) (Valley, 2003). Rather than reflecting primary source characteristics the O isotope data record the effect of open system processes prior to zircon crystallization. This is consistent with a mantle source derived magma, with intermediate $\delta^{18}O$ values (Fig. 8) assimilating a range of contaminants to drive $\delta^{18}O$ values to both higher and lower than the initial composition. This decoupling between O and Hf isotopes is comparable to previously reported whole-rock isotope characteristics (Brenna et al., 2015). These authors attributed large variations in $^{87}Sr/^{86}Sr$ coupled with relatively uniform $^{143}Nd/^{144}Nd$ to pre- or syn-eruptive hydrothermal alteration by sea water and high $^{87}Sr/^{86}Sr$ sediments. The Nd data, and zircon εHf_t presented here, indicate hydrothermally-altered crust incorporated into the magma was likely country rock from the same volcano-plutonic system rather than older continental crust. High, supra-mantle, $\delta^{18}O$ values are characteristic of continental crust, sedimentary or metasedimentary rocks and igneous rocks derived from these, e.g., S-type granites (Bindeman, 2008). Low, sub-mantle, $\delta^{18}O$ values, by contrast, are indicative of magmatic systems with a significant component of high temperature, > 300 °C, isotopically-light meteoric water, which may be derived from: hydrothermally-altered crust (e.g., Carley et al., 2014, 2017; Bindeman and Valley, 2001; Monani and Valley, 2001; Jo et al., 2016); or, high temperature hydrothermal fluid circulation into the magma body (e.g., Schmidt et al., 2013). Zircon with anomalously low $\delta^{18}O$ values can crystallize in any tectonomagmatic setting but are most typical in hot spots, rifts and nested caldera complexes (Troch et al., 2020). In these settings extensive fracture permeability allows for efficient hydrothermal alteration of country rock that may be subsequently assimilated by the magma. Assimilation of co-genetic hydrothermally-altered rocks will not usually affect magma major and trace element compositions but will be record in $\delta^{18}O$ (Troch et al., 2020).

We suggest contamination of mantle-derived magmas with a significant component of low temperature hydrothermally altered crust resulted in the high zircon $\delta^{18}O$ in the older plutonic syenites (OD-4 and OD-5; Fig. 8). This is consistent with whole-rock Sr isotopic compositions (Brenna et al., 2015). The younger syenite (OD-22) also records this contamination, but to a lesser extent, whereas this component is not apparent in the younger volcanic trachyte (OD-1) nor the hypabyssal rhyolite (OD-25). This may reflect interaction of early magma pulses with country rock forming a barrier at intrusion margins that prevented its assimilation by later pulses. In addition to the high $\delta^{18}O$ contaminant, all samples except the oldest syenite, also have anomalously low zircon $\delta^{18}O$ values indicating assimilation of a high-temperature hydrothermal component. Adding a significant component of liquid water to magma is physically complex. So, we suggest Oki-Dōzen low $\delta^{18}O$ values reflect that prior to zircon crystallization the magma assimilated country rock that was hydrothermally-altered by heated meteoric water. The low $\delta^{18}O$ rhyolite dike zircon values are consistent with extraction of evolved melt from the upper, shallow, region of a magma reservoir; this may be most likely to be adjacent to crust permeated and altered by meteoric hydrothermal fluids. The range of

This is the peer-reviewed, final accepted version for American Mineralogist, published by the Mineralogical Society of America.
The published version is subject to change. Cite as Authors (Year) Title. American Mineralogist, in press.
DOI: https://doi.org/10.2138/am-2021-7861. http://www.minsocam.org/

zircon oxygen isotope values indicates the country rock was heterogeneous with respect to $\delta^{18}O$ and contamination varied over time in each magmatic pulse as recorded in the compositional range of zircon crystallized in each sample. Within this compositional variation the youngest syenite and the trachyte are most similar, they are also closest in age.

MAGMA DIFFERENTIATION. Aside from the range in zircon $\delta^{18}O$ the most striking compositional feature of the Oki-Dōzen plutonic, hypabyssal and volcanic zircon compositions is the broad range of differentiation, inferred from the spread and inter-sample overlap of zircon Zr/Hf. However, before considering zircon Zr/Hf variations in detail, it is relevant to note the whole-rock Zr/Hf values ranges: syenites (26.6–22.2); rhyolite dike (32.5); and trachyte (55.3) (Fig. 10). Most crustal rocks have a Zr/Hf of ~35–40, i.e., near chondritic (Ahrens and Erlank, 1969; Hoskin and Schaltegger, 2003). Rhyolites and granites may have low Zr/Hf, 15-30, because of zircon fractionation depletion of Zr. This may be amplified by segregation of Zr-bearing major minerals such as amphibole, clinopyroxene and garnet (Bea et al., 2006). The syenites low whole-rock Zr/Hf values are, therefore, consistent with zircon fractionation (cf., Claiborne et al., 2006a) which typically provokes a drop off in whole-rock Zr/Hf in subduction-related systems at 76–79 wt% SiO_2 (Claiborne et al., 2006a). In the Oki-Dōzen system this occurred at ~60 wt% SiO_2 which may be a function of preferential accessory mineral segregation in lower viscosity alkaline magmas (cf., Giordano et al. 2004). On the other hand, elevated whole-rock Zr/Hf values in the trachyte suggest accumulation of scavenged xenocrystic and/or antecrystic zircon (cf., Claiborne et al., 2006a) enhanced, we suggest, by lack of amphibole fractionation in this sample. This is compatible with scatter observed in the trachyte age data (Fig. 4). The rhyolite whole-rock Zr/Hf range may result from a combination of depletion by zircon fractionation to below chondrite values and enrichment by zircon scavenged during ascent.

Differences in zircon trace element concentrations recorded in the plutonic, hypabyssal and volcanic samples indicate either: subtle variations in magma composition in the distinct pulses; or, differential incorporation of compatible trace elements at greater and shallower depth, perhaps because of variation in mineral stability related to crystallization temperature and pressure; or a combination of these. All three plutonic samples show typical trace element fractionation trends: Ti correlates positively with Zr/Hf (Fig. 5a), indicating more Ti was incorporated into zircon when the magmatic system was less-evolved and had fractionated less zircon. Amphibole, in which Ti and Sc are compatible, e.g., benmoreite Ti partition coefficient ~4 (Liotard et al., 1982), trachyte Sc partition coefficient ~15 (Lemarchand et al., 1987), may play a significant role in controlling the concentration of these elements in magmas and thus zircon. Amphibole is present as a minor phase in the syenites but only as rare, out of equilibrium, microphenocrysts in the trachyte (Fig. 2g). As noted above the syenite zircon have lower concentrations of Ti and Sc than the trachyte zircon. These compositional differences could result from more favorable P-T conditions for amphibole crystallization and fractionation at greater depth in the syenite magma thus depleting it in these elements relative to shallower stalling trachyte magma (cf., Barker et al., 2014). So, the two rock types having crystallized from the same, or a very similar, magma, is not precluded. Further evidence for amphibole in the fractionating assemblage includes: i) decoupling of zircon Ti concentrations from other zircon-compatible elements (e.g., U, Y, HFSE, MREE-HREE and LREE Ce (Fig. 5); ii) elevated U/Yb, in the syenites, relative to low ratios associated with amphibole-absent fractional crystallization in the trachyte (Fig. 5d) as a result of differences in amphibole U and Yb compatibility (cf., Brophy, 2009).

We suggest in the same way HREE-depletion in metamorphic zircon is indicative of associated garnet crystallization (e.g., Rubatto and Hermann, 2007), significant differences in zircon Sc and Ti concentrations in cogenetic magmatic suites trace amphibole fractionation (cf., Grimes et al., 2015). Depletion may occur synchronous with zircon crystallization, e.g., in subalkaline systems, or, prior to zircon crystallization if this occurs at a late stage, e.g., in alkaline systems such as Oki-Dōzen (cf., Boehnke et al., 2013; Gervasoni et al., 2016). Brenna et al. (2015) modeled fractional crystallization of the syenites with amphibole in the mineral assemblage from 57.5 wt% SiO_2, the syenites SiO_2 ranges from 61.5–63.8 wt%. Thus, the magma could already have been considerably depleted in Sc and Ti before zircon crystallized. In addition to primary magmatic zircon the trachyte also apparently scavenged zircon crystals raising whole-rock Zr/Hf; but this was apparently only from the shallow region unaffected by amphibole fractionation as all grains have high Sc and Ti (Fig. 5). The rhyolite dike also has one zircon grain with high Sc and Ti concentrations i.e., inferred to be shallow; we suggest this grain was scavenged en route to the surface**.** Identification of a control – amphibole fractionation - other than temperature on zircon Ti content highlights the importance of proceeding with caution when interpreting Ti-in-zircon thermometry in systems where amphibole is present.

As well as compositional differences between samples dictated by amphibole fractionation there are notable variations in the fractionation trends in the plutonic, hypabyssal and volcanic rocks. The constant Eu negative anomalies over the range of differentiation of the plutonic and hypabyssal zircon suggests Ca-rich plagioclase fractionation depleted the melt in Eu relative to other REE, prior to, but not during, zircon crystallization (cf., Hoskin and Ireland, 2000; Trail et al., 2012). In the more evolved rocks plagioclase was more Na^+-rich (Supplementary Material 2). Variable Eu anomalies at a given level of differentiation in the volcanic trachyte zircon, by contrast, is indicative of variable melt Eu depletion and thus Ca-rich plagioclase fractionation. This is consistent with the lack of a correlation between negative Eu and positive Ce anomalies because it indicates oxygen fugacity was not the sole control on these element concentrations. Melt Ce content, conversely, is not affected by crystallization of any major mineral so it is usually considered a more reliable indicator of melt oxidation state (Trail et al., 2012).

Element covariances are evident in some individual samples, e.g., syenite OD-5, absent in some e.g., rhyolite dike OD-25 and present, but to a lesser extent, in others e.g., the trachyte OD-1 (Fig. 5). Trends typical of suites of zircon crystals dominated by fractional crystallization are seen in syenites OD-5 and OD-22. Zircon compatible elements e.g., U and REE, correlate negatively with fractionation index Zr/Hf as a function of increased compatibility at lower temperature (Fig. 5) (cf., Storm et al., 2014; Troch et al., 2018). Notably, the typical igneous zircon trace element ratios indicate crystallization was not preceded by other Th-rich accessory minerals, e.g., monazite or allanite. The negative correlations, e.g., U and U/Yb and U/Th ratios in the syenites, albeit with varying gradients and concentrations, are dominated by the increase in zircon U concentration with differentiation (cf., Bea, 1996) (Fig. 5c–e). The syenites preserve early-formed through to late-stage, eutectic-like, zircon e.g., U content increases dramatically in OD-22 at evolved low Zr/Hf. Furthermore, a positive correlation is observed between $(Gd/Yb)_N$ and fractionation, Zr/Hf, in the syenites, but not in the trachyte nor the rhyolite (Fig. 5f). Decoupling of zircon MREE and HREE values can be explained by synchronous apatite fractionation. Prowatke and Klemme (2006) determined apatite MREE distribution coefficients (Kds ~3–15) are ~4–5 times greater than those for HREE (Kds ~1–3) for intermediate, albeit subalkaline, compositions. Accordingly, Zhang et al. (2020) invoked closed system apatite fractionation in granites to explain a drop in zircon Gd/Yb from 0.2 to 0.03, comparable to the range in the Oki-Dōzen syenite zircon: 0.18 to 0.05.

OKI-DŌZEN MAGMATIC SYSTEM MODEL

The key question asked above was whether plutons preserve i) erupted magma stalled and solidified at depth or ii) magma remaining following extraction of erupted melt. In the Oki-Dōzen rocks the plutonic syenites apparently preserve the former relationship with the volcanic trachyte and the latter with the hypabyssal rhyolite dike. By combining our new zircon age, isotopic and compositional data, major phase compositions and petrographic observations with conclusions of Brenna et al. (2015) we construct a model for the temporal evolution of the magmatic plumbing system (Fig. 11). Key aspects of this model include:

1. The magmatic source was uniform in terms of Hf isotopic signatures for the ~2 My duration of felsic volcanism and plutonism at Oki-Dōzen. The syenite, trachyte and rhyolite samples εHf_t values are within error ~3.6 to ~3.8 ± 0.63 indicating a common magma source. The felsic magmas differed, however, in their evolution. Variation can be seen in terms of fractionating assemblages: with or without amphibole; and significant spread in zircon trace element compositions e.g., Zr/Hf, Th/U, Sc and Ti indicating protracted fractionation in all but the dike. The degree, type and temperature of hydrothermally-altered continental crust assimilation varied between plutonic, volcanic and hypabyssal samples as recorded by zircon $\delta^{18}O$ heterogeneity. This may also reflect crystallization under variable, relatively oxidizing, conditions as a result of changes in magma volatile content as recorded in positive zircon Ce/Ce* anomalies in all samples (cf., Kelley and Cottrell, 2009).

2. Zircon ages and compositions track piecemeal assembly of the syenite body by incremental amalgamation of heterogenous melts as distinct magma pulses. The range of U-Th-Pb zircon ages from the syenite samples register prolonged zircon-saturation in the magmatic system. In detail, our new data corroborate formation of the pluton by at least two distinct pulses, deciphering differences not discernible in the whole-rock data. Preservation of the compositional variation in the zircon requires each magma pulse to have crystallized sufficiently prior to subsequent juxtaposition to prevent inter-pulse crystal-liquid mixing of minerals with different petrogenetic histories. differentiated Assemblage was controlled by flux of already magma between interconnected regions in the plumbing system. Notably, buoyant magma bodies with radii > 1 km can continue to rise to shallow depths even after solidification including in a brittle regime where they may induce faulting (Burov et al., 2003 and references therein).

3. Key petrological and compositional differences exist between the syenite and trachyte samples, particularly with respect to amphibole. Some syenite samples preserve cryptic evidence of stalling within the amphibole stability field (cf., Davidson et al., 2007) as recorded in low zircon Ti and Sc concentrations. This

is not so apparent, though, in other syenites and is absent in the trachyte. Thus, variable ascent and stalling of melt batches that ultimately formed the syenite pluton is highlighted. This is also evidenced by the large range in modeled temperatures and amphibole pressures for the syenite (800–1000ºC, 190–620 MPa) compared to the restricted range for the trachyte (910–970ºC, this work, and 210–390 MPa from Brenna et al., 2015). Therefore, the trachyte can be interpreted as a comparable magma to the syenites, either a tapped off portion of a syenite magma body or a separate magma body that did not stall so protractedly at depth.

4. The rhyolite dike represents a melt phase extracted from a crystallizing syenite body. Extraction of rhyolite melt from crystal mush is a balance between a magma body being i) sufficiently fractionated for the intercrystalline melt to be evolved and ii) sufficiently crystallized for significant convection to be suppressed but for melt still to be able to escape the crystal network. Both criteria are met at ~45% crystallization (Bachmann and Bergantz, 2004). The rhyolite dike apparently preserves this fortuitous moment in the magma development (cf., Deering et al., 2011). Intermediate composition batholiths often have an interstitial melt phase that is more SiO_2-rich than the whole-rock composition (e.g., Cashman and Blundy, 2000; Schmitt et al., 2003). The interstitial melt may separate and form a melt cap overlying the crystal-rich magma by some combination of: crystal settling (cf., Davis and Acrivos, 1985); compaction (McKenzie, 1984); or, gas-driven filter pressing in volatile-rich systems (Anderson et al., 1984). Zircon preferentially segregates into interstitial melt from remobilized crystal mushes compared to coeval major phases because of its small size (Claiborne et al., 2006b). Formation of the rhyolite in this way explains its whole-rock compositional gap with the syenites and trachytes. Also, when combined with zircon scavenging en route to the surface, it accounts for the broad age range and restricted level of fractionation. Dike zircon Zr/Hf (~80–60) overlap with the less evolved range of syenite zircon but notably do not contain any evolved grains, Zr/Hf (~60–40) (Fig. 5). The syenite OD-22 overlaps in age, within error, with the rhyolite dike, this combined with the zircon trace element compositional similarities identify it as a source candidate.

DOI: https://doi.org/10.2138/am-2021-7861. http://www.minsocam.org/

5. Zircon lacks intragrain compositional variability reflecting lack of fluctuation in magma composition during crystal growth. Brenna et al. (2015) related the nested core formation of silicic plutons surrounded by more primitive rocks to a dispersed, lower volume, plumbing system forming crustal barriers that hindered ascent of deep, primitive magma. The limited volcanic activity is consistent with a low-flux system in which magma stalled in the upper crust. Incremental pluton growth resulted with magma pulses preserved as discrete magmatic fractionation events and associated small- to moderate-scale, steady-state eruptions (cf., Claiborne et al. 2010; Mills and Coleman, 2013).

IMPLICATIONS

Combining zircon ages, trace element and isotopic data from coeval and co-genetic magmatic rocks can provide critical information about magmatic processes. Considering such data is an effective approach to investigate how plutons grow and whether plutonic rocks are i) counterpart or ii) residual to erupted magma volcanic rocks. Zircon records temporal and compositional subtleties that may be hidden in whole-rock data including broad plutonic-hypabyssal-volcanic connections and specific distinct magma pulses even in small, e.g., ~10 km surface expression diameter, plutons. Not every batch of magma sees the same path to a pluton. The crustal structure can form barriers resulting in variable magma stalling recorded by zircon. Intermediate magma at mid-crustal depths may fractionate to more evolved, silicic, less dense, syenitic magmas that could rise to shallower levels. By combining zircon Hf and O isotope data, primary source characteristics, εHf_t, may be unraveled from open system contamination, $\delta^{18}O$, of the magmatic system. Furthermore, zircon Sc and Ti concentrations can track amphibole crystallization and fractionation that lower melt concentrations of both elements, so less are incorporated into synchronously crystallized or later-formed zircon. In this way, these elements can be used as proxies for amphibole stability and thus depth of magma crystallization. This process could impact reliability of the Ti-in-zircon geothermometer in amphibole-bearing rocks.

Compositional similarities and differences between zircon crystallized in an intrusive and extrusive context link the Oki-Dōzen plutonic and volcanic rocks as different pulses of similar, counterpart, magma. The hypabyssal dike zircon, on the other hand, crystallized from a segregated magma. These deductions allow physical, thermal and compositional constraints to be placed at fixed points within the magmatic plumbing system evolution related to: magma source; melt segregation; and differentiation including assimilation and fractional crystallization processes.

The relation between the Oki-Dōzen plutonic-hypabyssal-volcanic rocks may be typical of low flux systems, e.g., non-plume ocean islands, rather than high flux plume-related ocean island systems, subduction-related transcrustal mush-melt reservoirs, large volume batholiths or supereruptions. Identification of episodic amalgamation of magma pulses, in any tectonomagmatic context, has important implications for determining potential fluxes and thus eruptible volumes of magma reservoirs.

ACKNOWLEDGEMENTS

Data collection for this project has received funding from the European Union's Horizon 2020 research and innovation programme under the Marie Skłodowska-Curie grant agreement No. 749611 (JHS) and Japan Society for the Promotion of Science postdoctoral fellowship #PE16724 (KJC). We also acknowledge funding from the Spanish grant CGL2017-84469-P. We are grateful to T. Sato (JAMSTEC), R. Senda (Kyushu University) and G. Cooper (Cardiff University) for technical assistance and valuable discussions. Callum Hetherington is thanked for editorial handling and detailed comments that significantly improved the manuscript. We are much obliged to reviewers Marco Brenna and John Encarnacion for the time and effort they took to help us improve the clarity and rigor of our interpretations. This is the IBERSIMS publication Nº 87.

REFERENCES

Allibon, J., Bussy, F., Lewin, E., and Darbellay, B. (2011) The tectonically controlled emplacement of a vertically sheeted gabbro-pyroxenite intrusion: feeder-zone of an ocean-island volcano (Fuerteventura, Canary Islands) Tectonophysics, 500, 78–97.

Anderson Jr, A.T., Swihart, G.H., Artioli, G., and Geiger, C.A. (1984) Segregation vesicles, gas filter-pressing, and igneous differentiation. The Journal of Geology, 92, 55–72.

Ahrens, L.H., and Erlank, A.J. (1969) Hafnium. In Editor: Wedepohl K.H. Handbook of Geochemistry, 2, 5, B–O, Springer, Berlin.

Bachmann, O., and Bergantz, G.W. (2004) On the origin of crystal-poor rhyolites: extracted from batholithic crystal mushes. Journal of Petrology, 45, 1565–1582.

Barker, S.J., Wilson, C.J.N., Smith, E.G., Charlier, B.L.A., Wooden, J.L., Hiess, J., and Ireland, T.R. (2014) Post-supereruption magmatic reconstruction of Taupo volcano (New Zealand), as reflected in zircon ages and trace elements. Journal of Petrology, 55, 1511–1533.

Barth, A.P., Feilen, A.D.G., Yager, S.L., Douglas, S.R., Wooden, J.L., Riggs, N.R., and Walker, J.D. (2012) Petrogenetic connections between ash-flow tuffs and a granodioritic to granitic intrusive suite in the Sierra Nevada arc, California. Geosphere, 8, 250–264.

Bea, F. (1996) Residence of REE, Y, Th and U in granites and crustal protoliths; implications for the chemistry of crustal melts. Journal of Petrology, 37, 521–552.

Bea, F., Montero, P., and Ortega Huertas, M. (2006) A LA-ICP-MS evaluation of Zr reservoirs in common crustal rocks: Implications for Zr and Hf geochemistry, and zircon-forming processes. The Canadian Mineralogist, 44, 693-714.

Bindeman, I.N. (2008) Oxygen isotopes in mantle and crustal magmas as revealed by single crystal analysis. Reviews in Mineralogy and Geochemistry, 69, 445–478.

Bindeman, I.N., and Valley, J.W. (2001) Low-δ18O rhyolites from Yellowstone: Magmatic evolution based on analyses of zircons and individual phenocrysts. Journal of Petrology, 42, 1491–1517.

Boehnke, P., Watson, E.B., Trail, D., Harrison, T.M. and Schmitt, A.K. (2013) Zircon saturation re-revisited. Chemical Geology. 351, 324–334.

Brenna, M., Nakada, S., Miura, D., Toshida, K., Ito, H., Hokanishi, N., and Nakai, S.I. (2015) A trachyte–syenite core within a basaltic nest: filtering of primitive injections by a multi-stage magma plumbing system (Oki-Dōzen, south-west Japan) Contributions to Mineralogy and Petrology, 170, 22–43.

Brophy, J.G. (2009) La–SiO2 and Yb–SiO2 systematics in mid-ocean ridge magmas: implications for the origin of oceanic plagiogranite. Contributions to Mineralogy and Petrology 158, 99-111.

Burov, E., Jaupart, C., and Guillou-Frottier, L. (2003) Ascent and emplacement of buoyant magma bodies in brittle-ductile upper crust. Journal of Geophysical Research, 108, 2177–2197.

Caricchi, L., Simpson, G., and Schaltegger, U. (2014) Zircons reveal magma fluxes in the Earth's crust. Nature, 511, 457–461.

Carley, T.L., Miller, C.F., Wooden, J.L., Padilla, A.J., Schmitt, A.K., Economos, R.C., and Jordan, B. T. (2014) Iceland is not a magmatic analog for the Hadean: Evidence from the zircon record. Earth and Planetary Science Letters, 405, 85–97.

Carley, T.L., Miller, C.F., Sigmarsson, O., Coble, M.A., Fisher, C.M., Hanchar, J.M., and Economos, R.C. (2017) Detrital zircon resolve longevity and evolution of silicic magmatism in extinct volcanic centers: A case study from the East Fjords of Iceland. Geosphere, 13, 1640–1663.

Cashman, K.V., and Blundy, J.D. (2000) Degassing and crystallization of ascending andesite and dacite. Philosophical Transactions of the Royal Society of London. Series A: Mathematical, Physical and Engineering Sciences, 358, 1487–1513.

Cashman, K.V., Sparks, R.S.J., and Blundy, J.D. (2017) Vertically extensive and unstable magmatic systems: a unified view of igneous processes. Science, 355, eaag3055

Chamberlain, K.J., Wilson, C.J., Wooden, J.L., Charlier, B.L., and Ireland, T.R. (2014) New perspectives on the Bishop Tuff from zircon textures, ages and trace elements. Journal of Petrology, 55, 395–426.

Choi, H.O., Choi, S.H., Lee, D.C., and Kang, H.C. (2013) Geochemical evolution of basaltic volcanism within the tertiary basins of southeastern Korea and the opening of the East Sea (Sea of Japan). Journal of Volcanology and Geothermal Research, 249, 109-122.

Chu, M.F., Wang, K.L., Griffin, W.L., Chung, S.L., O'Reilly, S.Y., Pearson, N.J., and Iizuka, Y. (2009) Apatite composition: tracing petrogenetic processes in Transhimalayan granitoids. Journal of Petrology, 50, 1829–1855.

Claiborne, L.L., Miller, C.F., Walker, B.A., Wooden, J.L., Mazdab, F.K., and Bea, F. (2006a) Tracking magmatic processes through Zr/Hf ratios in rocks and Hf and Ti zoning in zircons: an example from the Spirit Mountain batholith, Nevada. Mineralogical Magazine, 70, 517–543.

Claiborne, L.L., Furbish D.J., and Miller C.F. (2006b) Determining mechanics of segregating small crystals from melt using modeling and SHRIMP-RG trace element analysis of zircons: An example from the Spirit Mountain Batholith, Nevada: Eos Transactions of the American Geophysical Union, 87, V54B–02.

Claiborne, L.L., Miller, C.F., Flanagan, D.M., Clynne, M.A., and Wooden, J.L. (2010) Zircon reveals protracted magma storage and recycling beneath Mount St. Helens. Geology, 38, 1011–1014.

Cluzel, D., and Meffre, S. 2019. In search of Gondwana heritage in the Outer Melanesian Arc: no pre-upper Eocene detrital zircons in Viti Levu river sands (Fiji Islands). Australian Journal of Earth Sciences, 66, 265–27.

Coleman, D.S., Mills, R.D., and Zimmerer, M.J. (2016) The pace of plutonism. Elements, 12, 97–102.

Davidson, J., Turner, S., Handley, H., Macpherson, C., and Dosseto, A. (2007) Amphibole "sponge" in arc crust? Geology, 35, 787–790.

Davis, R.H., and Acrivos, A. (1985) Sedimentation of noncolloidal particles at low Reynolds numbers. Annual Review of Fluid Mechanics, 17, 91–118.

Deering, C.D., Cole, J.W. and Vogel, T.A. (2011) Extraction of crystal-poor rhyolite from a hornblende-bearing intermediate mush: a case study of the caldera-forming Matahina eruption, Okataina volcanic complex. Contributions to Mineralogy and Petrology, 161, 129–151.

Deering, C.D., Keller, B., Schoene, B., Bachmann, O., Beane, R., and Ovtcharova, M. (2016) Zircon record of the plutonic-volcanic connection and protracted rhyolite melt evolution. Geology, 44, 267–270.

Farina, F., Stevens, G., and Villaros, A. (2012) Multi-batch, incremental assembly of a dynamic magma chamber: the case of the Peninsula pluton granite (Cape Granite Suite, South Africa). Mineralogy and Petrology, 106, 193-216.

Faure, G., (1986) Principles of Isotope Geology (2nd edn). 589 pp; Wiley, New York.

Ferry, J.M., and Watson, E.B. (2007) New thermodynamic models and revised calibrations for the Ti-in-zircon and Zr-in-rutile thermometers. Contributions to Mineralogy and Petrology, 154, 429–437.

Gelman, S.E., Deering, C.D., Bachmann, O., Huber, C., and Gutierrez, F.J. (2014) Identifying the crystal graveyards remaining after large silicic eruptions. Earth and Planetary Science Letters, 403, 299–306.

Gervasoni, F., Klemme, S., Rocha-Júnior ERV and Berndt, J. (2016) Zircon saturation in silicate melts: a new and improved model for aluminous and alkaline melts. Contributions to Mineralogy and Petrology, 171, 21–32.

Ghiorso, M.S., and Gualda, G.A. (2013) A method for estimating the activity of titania in magmatic liquids from the compositions of coexisting rhombohedral and cubic iron–titanium oxides. Contributions to Mineralogy and Petrology, 165, 73–81.

Giordano, D., Romano, C., Papale, P., and Dingwell, D.B. (2004) The viscosity of trachytes, and comparison with basalts, phonolites, and rhyolites. Chemical Geology 213,49–61.

Glazner, A.F., Bartley, J.M., Coleman, D.S., Gray, W., and Taylor, R.Z. (2004) Are plutons assembled over millions of years by amalgamation from small magma chambers? Geological Society of America Today, 14, 4–12.

Glazner, A.F., Coleman, D.S., and Mills, R.D. (2015) The volcanic-plutonic connection. In Editors: C. Breitkreuz, and S. Rocchi, Physical Geology of shallow magmatic systems, Dykes; Sills and Laccoliths., p. 61–82, Springer, New York.

Gudmundsson, A. (2012) Magma chambers: Formation, local stresses, excess pressures, and compartments. Journal of Volcanology and Geothermal Research, 237, 19–41.

Grimes, C.B., Wooden, J.L., Cheadle, M.J., and John, B.E. (2015) "Fingerprinting" tectono-magmatic provenance using trace elements in igneous zircon. Contributions to Mineralogy and Petrology, 170, 46.

Hawkesworth, C.J., Dhuime, B., Pietranik, A.B., Cawood, P.A., Kemp A.I.S. and Storey, C.D. (2010) The generation and evolution of the continental crust. Journal of the Geological Society, 167, 229–248.

Hayden, L.A., and Watson, E.B. (2007) Rutile saturation in hydrous siliceous melts and its bearing on Ti-thermometry of quartz and zircon. Earth and Planetary Science Letters, 258, 561–568.

Hofmann, A.W. (1988) Chemical differentiation of the Earth: the relationship between mantle, continental crust, and oceanic crust. Earth and Planetary Science Letters, 90, 297–314.

Hoskin, P.W.O., and Ireland, T.R. (2000) Rare earth element chemistry of zircon and its use as a provenance indicator. Geology, 28, 627-630.

Hoskin, P.W.O., (2005) Trace-element composition of hydrothermal zircon and the alteration of Hadean zircon from the Jack Hills, Australia. Geochimica et Cosmochimica Acta, 69, 637-664.

This is the peer-reviewed, final accepted version for American Mineralogist, published by the Mineralogical Society of America.
The published version is subject to change. Cite as Authors (Year) Title. American Mineralogist, in press.
DOI: https://doi.org/10.2138/am-2021-7861. http://www.minsocam.org/

Hoskin, P.W.O., and Schaltegger, U. (2003) The composition of zircon and igneous and metamorphic petrogenesis. Reviews in Mineralogy and Geochemistry. 53, 27–62.

Humphreys, M.C., Cooper, G.F., Zhang, J., Loewen, M., Kent, A.J., Macpherson, C.G., and Davidson, J.P. (2019) Unravelling the complexity of magma plumbing at Mount St. Helens: a new trace element partitioning scheme for amphibole. Contributions to Mineralogy and Petrology, 174, 9.

Jiang, W.C., Lia, H., Evans, N.J., and Wua, J.H. (2019) Zircon records multiple magmatic-hydrothermal processes at the giant Shizhuyuan W–Sn–Mo–Bi polymetallic deposit, South China. Ore Geology Reviews, 115, 103160.

Jo, H. J., Chang-sik Cheong, A., Ryu, J.S., Kim, N., Yi, K., Jung, H., and Li, X H. (2016) In-situ oxygen isotope records of crustal self-cannibalization selectively captured by zircon crystals from high-δ^{26}Mg granitoids. Geology, 44, 339–342.

Kaneko, N. (1991) Petrology of Oki-Dōzen volcano. Part I. Petrography and major and trace element compositions. Journal of Mineralogy, Petrology and Economic Geology, 86, 140–159.

Keller, C.B., Schoene, B., Barboni, M., Samperton, K.M., and Husson, J.M. (2015) Volcanic–plutonic parity and the differentiation of the continental crust. Nature, 523, 301–307.

Kelley, K.A., and Cottrell, E. (2009) Water and the oxidation state of subduction zone magmas. Science, 325, 605–607.

Leake, B.E., Woolley, A.R., Arps, C.E., Birch, W.D., Gilbert, M.C., Grice, J.D., and Linthout, K. (1997) Nomenclature of amphiboles; report of the Subcommittee on Amphiboles of the International Mineralogical Association Commission on new minerals and mineral names. Mineralogical magazine, 61, 295–310.

Leake, B.E., Woolley, A.R., Birch, W.D., Burke, E.A., Ferraris, G., Grice, J.D., and Stephenson, N. C. (2003) Nomenclature of amphiboles: additions and revisions to the International Mineralogical Association's 1997 recommendations. The Canadian Mineralogist, 41, 1355–1362.

Lemarchand, F., Benoit, V., and Calais, G. (1987) Trace element distribution coefficients in alkaline series. Geochimica et Cosmochimica Acta, 51, 1,071–1,081.

Liotard, J.M., Dupuy, C., Dostal, J., and Cornen, G. (1982) Geochemistry of the volcanic island of Annobon, Gulf of Guinea, Chemical Geology, 35, 115–128.

Lipman, P.W. (1984) The roots of ash flow calderas in western North America: windows into the tops of granitic batholiths. Journal of Geophysical Research: Solid Earth, 89 (B10), 8801–8841.

Lipman, P.W., and Bachmann, O. (2015) Ignimbrites to batholiths: Integrating perspectives from geological, geophysical, and geochronological data. Geosphere, 11, 705–743.

Lundstrom, C. C., and Glazner, A. F. (2016) Silicic magmatism and the volcanic–plutonic connection. Elements, 12, 91–96.

Masotta, M., Mollo, S., Freda, C., Gaeta, M., and Moore, G. (2013) Clinopyroxene–liquid thermometers and barometers specific to alkaline differentiated magmas. Contributions to Mineralogy and Petrology, 166, 1545–1561.

McDonough, W.F., and Sun, S.S. (1995) The composition of the Earth. Chemical Geology, 120, 223–253.

McKenzie, D. (1984) The generation and compaction of partially molten rock. Journal of Petrology, 25, 713-765.

Metcalf, R.V. (2004) Volcanic-plutonic links, plutons as magma. Transactions of the Royal Society of Edinburgh: Earth Sciences, 95, 357–374.

Michel, J., Baumgartner, L., Putlitz, B., Schaltegger, U., and Ovtcharova, M. (2008) Incremental growth of the Patagonian Torres del Paine laccolith over 90 ky. Geology, 36, 459-462.

Miller, C.F., Furbish, D.J., Walker, B.A., Claiborne, L.L., Koteas, G.C., Bleick, H.A., and Miller, J.S. (2011) Growth of plutons by incremental emplacement of sheets in crystal-rich host: Evidence from Miocene intrusions of the Colorado River region, Nevada, USA. Tectonophysics, 500, 65–77.

Mills, R.D., and Coleman, D.S. (2013) Temporal and chemical connections between plutons and ignimbrites from the Mount Princeton magmatic center. Contributions to Mineralogy and Petrology, 165, 961–980.

Molina, J.F., Moreno, J.A., Castro, A., Rodríguez, C., and Fershtater, G.B. (2015) Calcic amphibole thermobarometry in metamorphic and igneous rocks: New calibrations based on plagioclase/amphibole Al-Si partitioning and amphibole/liquid Mg partitioning. Lithos, 232, 286–305.

Monani, S., and Valley, J.W. (2001) Oxygen isotope ratios of zircon: magma genesis of low $\delta^{18}O$ granites from the British Tertiary Igneous Province, western Scotland. Earth and Planetary Science Letters, 184, 377–392.

Morris, P.A. (1986) Geochemistry of some Miocene to Quaternary igneous rocks bordering an ensialic marginal basin—an example from eastern Shimane Prefecture and Oki Dozen Island, Southwest Japan. Memoirs of the Faculty of Science of Shimane University 20, 15–133.

Morris, P.A., Itaya, T., Watanabe, T., and Yamauchi, S. (1990) Potassium/argon ages of Cenozoic igneous rocks from eastern Shimane Prefecture—Oki Dozen Island, Southwest Japan and the Japan Sea opening. Journal of Southeast Asian Earth Sciences, 4, 125–131.

Morris P.A., Itaya T., Iizumi S., Kagami H., Watling R.J., and Murakami H. (1997) Age relations and petrology of alkalic igneous rocks from Oki Dozen, Southwest Japan. Geochemical Journal, 31, 135–154.

Naemura, M., and Shimada, I. (1984) Neogene Tertiary of Nishino-shima, Dōzen, Oki Islands. Geological Reports of Shimane University, 3, 155–160.

Ni, Z., Arevalo, R., Piccoli, P., and Reno, B.L. (2020) A novel approach to identifying mantle-equilibrated zircon by using trace element chemistry. Geochemistry, Geophysics, Geosystems, 21, e2020GC009230.

Otofuji, Y-I., Matsuda, T., and Nohda, S. (1985) Paleomagnetic evidence for the Miocene counter-clockwise rotation of Northeast Japan—rifting process of the Japan Arc. Earth and Planetary Science Letters 75, 265–277.

Pitcher, W.S. (1979) Comments on the geological environments of granites. In M.P. Atherton and J. Tarney, Eds. Origin of granite batholiths, 1–8, Birkhäuser, Boston.

Putirka, K.D. (2008) Thermometers and barometers for volcanic systems. Reviews in Mineralogy and Geochemistry, 69, 61–120.

Prowatke, S., and Klemme, S. (2006) Trace element partitioning between apatite and silicate melts. Geochimica et Cosmochimica Acta 70, 4513-4527.

Reid, M.R., Vazquez, J.A., and Schmitt, A.K. (2011) Zircon-scale insights into the history of a Supervolcano, Bishop Tuff, Long Valley, California, with implications for the Ti-in-zircon geothermometer. Contributions to Mineralogy and Petrology, 161, 293–311.

Ridolfi, F., and Renzulli, A. (2012) Calcic amphiboles in calc-alkaline and alkaline magmas: thermobarometric and chemometric empirical equations valid up to 1,130° C and 2.2 GPa. Contributions to Mineralogy and Petrology, 163, 877–895.

Ridolfi, F., Renzulli, A., and Puerini, M. (2010) Stability and chemical equilibrium of amphibole in calc-alkaline magmas: an overview, new thermobarometric formulations and application to subduction-related volcanoes. Contributions to Mineralogy and Petrology, 160, 45–66.

Rubatto, D., and Hermann, J. (2007) Experimental zircon/melt and zircon/garnet trace element partitioning and implications for the geochronology of crustal rocks. Chemical Geology, 241, 38–61.

Scarrow, J.H., Molina, J.F., Bea, F., and Montero, P. 2009. Within-plate calc-alkaline rocks: Insights from alkaline mafic magma–peraluminous crustal melt hybrid appinites of the Central Iberian Variscan continental collision. Lithos, 110, 50–64.

Schiller, D., and Finger, F. (2019) Application of Ti-in-zircon thermometry to granite studies: problems and possible solutions. Contributions to Mineralogy and Petrology, 174, 51.

Schmidt, C., Steele-MacInnis, M., Watenphul, A., and Wilke, M. (2013) Calibration of zircon as a Raman spectroscopic pressure sensor to high temperatures and application to water-silicate melt systems. American Mineralogist, 98, 643–650.

Schmitt, A.K., Grove, M., Harrison, T.M., Lovera, O., Hulen, J., and Walters, M. (2003) The Geysers-Cobb Mountain Magma System, California (Part 2): Timescales of pluton emplacement and implications for its thermal history. Geochimica et Cosmochimica Acta, 67, 3443–3458.

Shane, P., and Smith, V.C. (2013) Using amphibole crystals to reconstruct magma storage temperatures and pressures for the post-caldera collapse volcanism at Okataina volcano. Lithos, 156, 159-170.

Storm, S., Schmitt, A.K., Shane, P., and Lindsay, J.M. (2014) Zircon trace element chemistry at sub-micrometer resolution for Tarawera volcano, New Zealand, and implications for rhyolite magma evolution. Contributions to Mineralogy and Petrology, 167, 1–19.

Tera, F., and Wasserburg, G. J. (1972) U-Th-Pb systematics in lunar highland samples from the Luna 20 and Apollo 16 missions. Earth and Planetary Science Letters, 17, 36–51.

Thornber, C.R., Pallister, J.S., Lowers, H.A., Rowe, M.C., Mandeville, C.W., and Meeker, G.P. (2008) Chemistry, mineralogy, and petrology of amphibole in Mount St. Helens 2004–2006 dacite. In Editors: Sherrod, D.R., Scott, W.E., and Stauffer, P.H., A volcano rekindled, 2004-2006. U.S. Geological Survey Professional Paper 1750.

Tiba, T. (1986) Alkalic volcanism at Oki-Dōzen. Memoirs of the National Science Museum, Tokyo, 19, 19–27.

Tiba, T., Kaneko, N., and Kano K. (2000) Geology of the Uragō District - with 1:50,000 Geological Sheet Map. (in Japanese with English abstract).

Trail, D., Watson, E.B., and Tailby, N.D. (2012) Ce and Eu anomalies in zircon as proxies for the oxidation state of magmas. Geochimica et Cosmochimica Acta, 97, 70–87.

Troch, J., Ellis, B.S., Schmitt, A.K., Bouvier, A.S., and Bachmann, O. (2018) The dark side of zircon: textural, age, oxygen isotopic and trace element evidence of fluid saturation in the subvolcanic reservoir of the Island Park-Mount Jackson Rhyolite, Yellowstone (USA) Contributions to Mineralogy and Petrology, 173, 54–71.

Troch, J., Ellis, B.S., Harris, C., Bachmann, O., and Bindeman, I. N. (2020) Low-$\delta^{18}O$ silicic magmas on Earth: A review. Earth-Science Reviews, 103299, https://doi.org/10.1016/j.earscirev.2020.103299.

Valley, J.W. (2003) Oxygen isotopes in zircon. Reviews in Mineralogy and Geochemistry, 53, 343–385.

Van de Flierdt, T., Goldstein, S.L., Hemming, S.R., Roy, M., Frank, M., and Halliday, A.N. (2007) Global neodymium–hafnium isotope systematics—revisited. Earth and Planetary Science Letters, 259, 432–441.

Wada, Y., Itaya, T., and Ui, T. (1990) K–Ar ages of Oki-Dozen and Tango dike Swarms, Western Honshu, Japan. Bulletin of the Volcanological Society of Japan, 35, 217–229.

Watson, E.B. and Harrison, T.M. (1983) Zircon saturation revisited: temperature and composition effects in a variety of crustal magma types. Earth and Planetary Science Letters, 64, 295–304.

Watson, E.B., Wark, D.A., and Thomas, J.B. (2006) Crystallization thermometers for zircon and rutile. Contributions to Mineralogy and Petrology, 151, 413.

Yan, L.L., He, Z.Y., Beier, C., and Klemd, R. (2018) Zircon trace element constrains on the link between volcanism and plutonism in SE China. Lithos, 320, 28–34.

Yan, L.L, He. Z.Y., Klemd, R., Beier, C., and Xu X.S. (2020) Tracking crystal-melt segregation and magma recharge using zircon trace element data. Chemical Geology, 542, 119596.

Zhang, W. Jiang, S.Y., Gao, T.S., Ouyang, Y.P., and Zhang, D. (2020) The effect of magma differentiation and degassing on ore metal enrichment during the formation of the world-class Zhuxi W-Cu skarn deposit: Evidence from U-Pb ages, Hf isotopes and trace elements of zircon, and whole-rock geochemistry. Ore Geology Review, 127, 103801.

Zhong, S., Seltmann, R., Qu, H., and Song, Y. (2019) Characterization of the zircon Ce anomaly for estimation of oxidation state of magmas: a revised Ce/Ce* method. Mineralogy and Petrology, 113, 755–763.

FIGURE CAPTIONS

Figure 1. Geological map of Oki-Dōzen, Japan Sea, modified from Tiba et al. (2000), showing the extent of the Miocene Ōyama syenite pluton, Takuhiyama pyroclastic cone cut by rhyolite dikes, trachyte series, sedimentary formation and the younger Pliocene Uzuka basalt series. Inset: map of the regional tectonic setting of Oki-Dōzen in the Japan arc. The sampling locations are marked with stars.

Figure 2. a. View of the Dōzen Islands looking north from Mt. Akahage, Chiburijima Island (from http://www.oki-geopark.jp/en/episode/geohistory/stage3/dozen-caldera/); b. Field photograph of the Takuhiyama pyroclastic cone trachyte, OD-1, cut by an outcrop of yellow rhyolite dike, OD-25, ~8 m wide, contact marked by dashed line; c. Field photograph of the Ʊya a syenite, OD-4, outcrop width ~15 m; d. Hand specimen close up of the volcanic trachyte, OD-1, black and white centimeter scale; e. Hand specimen close up of the rhyolite dike, OD-25, black and white centimeter scale, contact with trachyte marked by dashed line; f. Hand specimen close up of the Ʊya a syenite, OD-22, black and white centimeter scale; g. Photomicrograph of the volcanic trachyte, OD-1, field of view 0.7 cm, plane polarized light; h. Photomicrograph of rhyolite dike, OD-25, field of view 0.7 cm, plane polarized light; i. Photomicrograph of Ʊy ma syenite, OD-4, field of view 0.7 cm, plane polarized light, euhedral alkali feldspar outlined by dashed line. Mineral and groundmass abbreviations: afs – alkali feldspar; amp – amphibole; bt – biotite; dq-amp – disequilibrium amphibole; gm – groundmass; ox- Fe-Ti oxides; qz – quartz; zrn – zircon.

Figure 3. Whole-rock major and trace element data plots for the trachtye, rhyolite and syenite from the present study, major elements are expressed in weight percent, trace elements in ppm. The range of compositions of the different rock types from the literature are marked as shaded fields. Literature data from Brenna et al. (2015). a. Total alkalis versus silica diagram, note the alkaline character of all the rock types.

Alk - alkaline, Ca+Th - calc-alkaline and tholeiitic sub-alkaline field; b. Alkalis ($Na_2O + K_2O$), magnesium (MgO) and iron (FeO_t + MnO) plot; c. Al_2O_3 versus SiO_2; d. TiO_2 versus SiO_2; e. Sc versus SiO_2; f. Zr versus SiO_2; g. NMORB-normalized trace element plots, normalization values from Hofmann (1988); h. Chondrite-normalized rare earth element plots, normalization values from McDonough and Sun (1995).

Figure 4. Histograms and kernel-density curves of the zircon U-Th-Pb dates, inset boxes: mean $^{206}Pb/^{238}U$ (207-corrected) dates, errors and MSWD; gray vertical dashed lines mark the mean $^{206}Pb/^{238}U$ dates and the gray shadow bars the 1σ error, a. broad orange shadow and c.–e. broad red shadow mark the range of previously published ages (Brenna et al., 2015 and references therein) (left-hand side). Wetherill concordia plots that show common-lead discordia and lower interception date for each of the studied samples (right-hand side).

Figure 5. Zircon trace element concentrations and element ratios versus differentiation index Zr/Hf, a. Ti, b. Sc, c. U, d. U/Yb, e. U/Th, f. $(Gd/Yb)_N$. All elements expressed in ppm. Symbols as in Fig. 3.

Figure 6. Zircon chondrite-normalized rare earth element plots. All samples show a pronounced positive anomaly in Ce and a negative anomaly in Eu, normalization values of McDonough and Sun (1995). Symbols as in Fig. 3.

Figure 7. Tectonomagmatic discrimination diagrams based on zircon compositions. a. U/Yb versus Nb/Yb; b. Sc/Yb versus Nb/Yb; c. U/Yb versus Hf; d. Ti versus Sc/Yb; e. Th versus U. Fields from Grimes et al. (2015) and Cluzel and Meffre (2019). All elements expressed in ppm. Symbols as in Fig. 3.

Figure 8. Zircon $\delta^{18}O$ values. The grey horizontal band marks the compositional range typical of zircon crystallized from mantle-derived magmas (Valley, 2003). Note that values of $\delta^{18}O$ higher than this are typical of magmas with a component of continental crust that has some component of low temperature water and lower $\delta^{18}O$ values of magmatic systems with a significant component of high temperature hydrothermally altered crust. The 2σ errors on the $\delta^{18}O$ values are within the symbol size, see Supplementary Material 3 for details. Symbols as in Fig. 3.

Figure 9. Modeled magmatic temperatures using: amphibole-melt thermometry (triangles), amphibole composition thermometry (diamonds), alkali feldspar-melt thermometry (rectangles), plagioclase-melt thermometry (circle s) and Ti-in-zircon thermometry at varying $a\mathrm{TiO_2}$ (dashed lines and crosses). The symbols represent average temperature modeled, with the range in modeled temperature represented by the bars in the same colors. For references to calibrations used see 'Intensive Variables' section.

Figure 10. Whole-rock Zr/Hf versus SiO_2. Note the displacement of the syenites to Zr/Hf values lower than chondrite - indicative of zircon fractionation - and the elevated values of the trachyte - suggesting zircon accumulation.

Figure 11. Model of the evolution of the Oki-Dōzen magmatic system over time, not to vertical scale, from our data on the central felsic complex, and the work of Brenna et al. (2015) for the peripheral volcanism. a. 7.5–6.4 Ma highlights variable depth stalling of magma pulses and crystallization of compositionally diverse zircon from a single magmatic body b. 6.4–5.2 Ma highlights pluton formation by amalgamation of distinct magma pulses and the development of the hypabyssal and volcanic magmatic plumbing system. Key aspects of the system are labeled with numbers relating to the relevant section in the 'Model of the Oki-Dōzen

magmatic system' section of the text. Blue-grey areas represent non-uniform $\delta^{18}O$ crust- with darker areas reflecting high $\delta^{18}O$ areas, and lighter areas low $\delta^{18}O$ areas. The smaller dark gray zircon has high Zr/Hf and the smaller white zircon low Zr/Hf.

DOI: https://doi.org/10.2138/am-2021-7861. http://www.minsocam.org/

SUPPLEMENTARY MATERIALS

1- Data, methods details, precision and accuracy data

2- Major phase major and trace element compositions

3- Zircon CL images, trace elements, isotopes and text for interpretation

Fig. 1

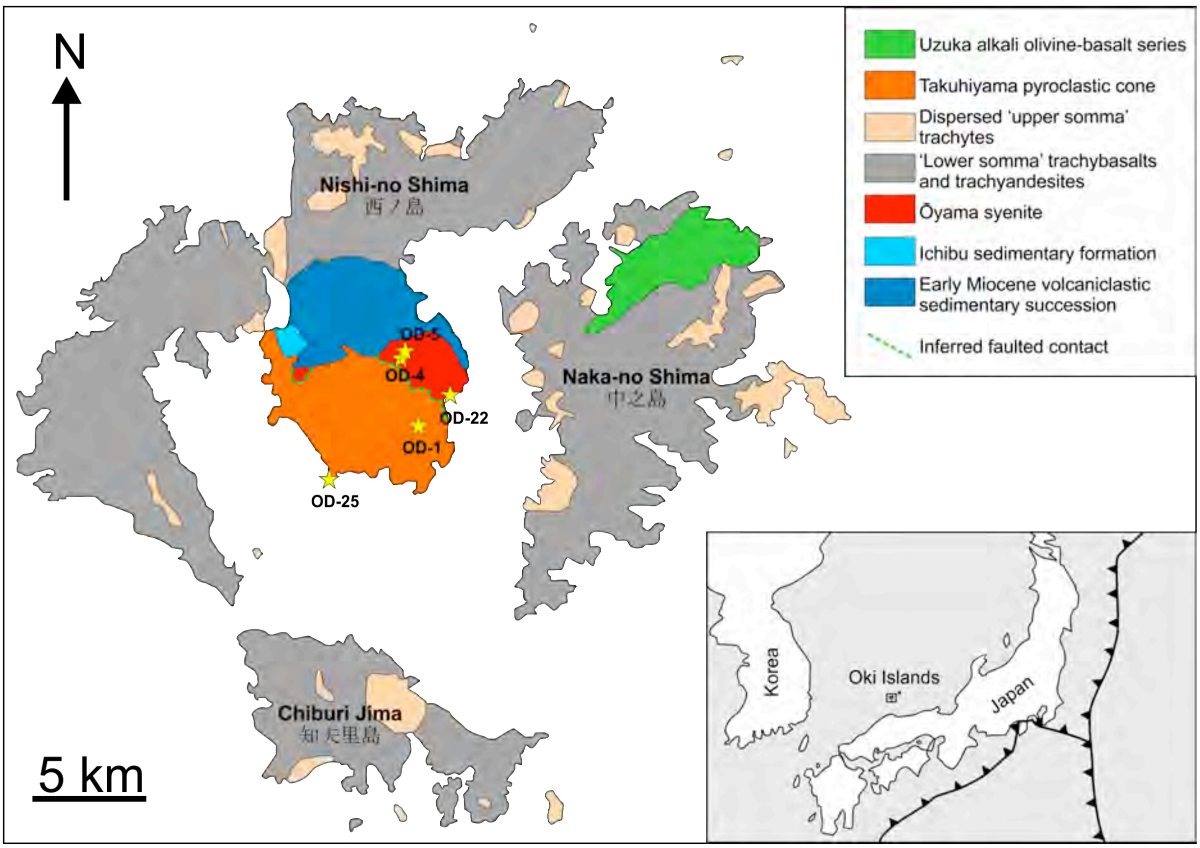
N
Nishi-no Shima
西ノ島
Naka-no Shima
中之島
Chiburi Jima
知夫里島
OD-5
OD-4
OD-22
OD-1
OD-25
5 km
Uzuka alkali olivine-basalt series
Takuhiyama pyroclastic cone
Dispersed 'upper somma' trachytes
'Lower somma' trachybasalts and trachyandesites
Ōyama syenite
Ichibu sedimentary formation
Early Miocene volcaniclastic sedimentary succession
Inferred faulted contact
Korea
Oki Islands
Japan

Fig. 2

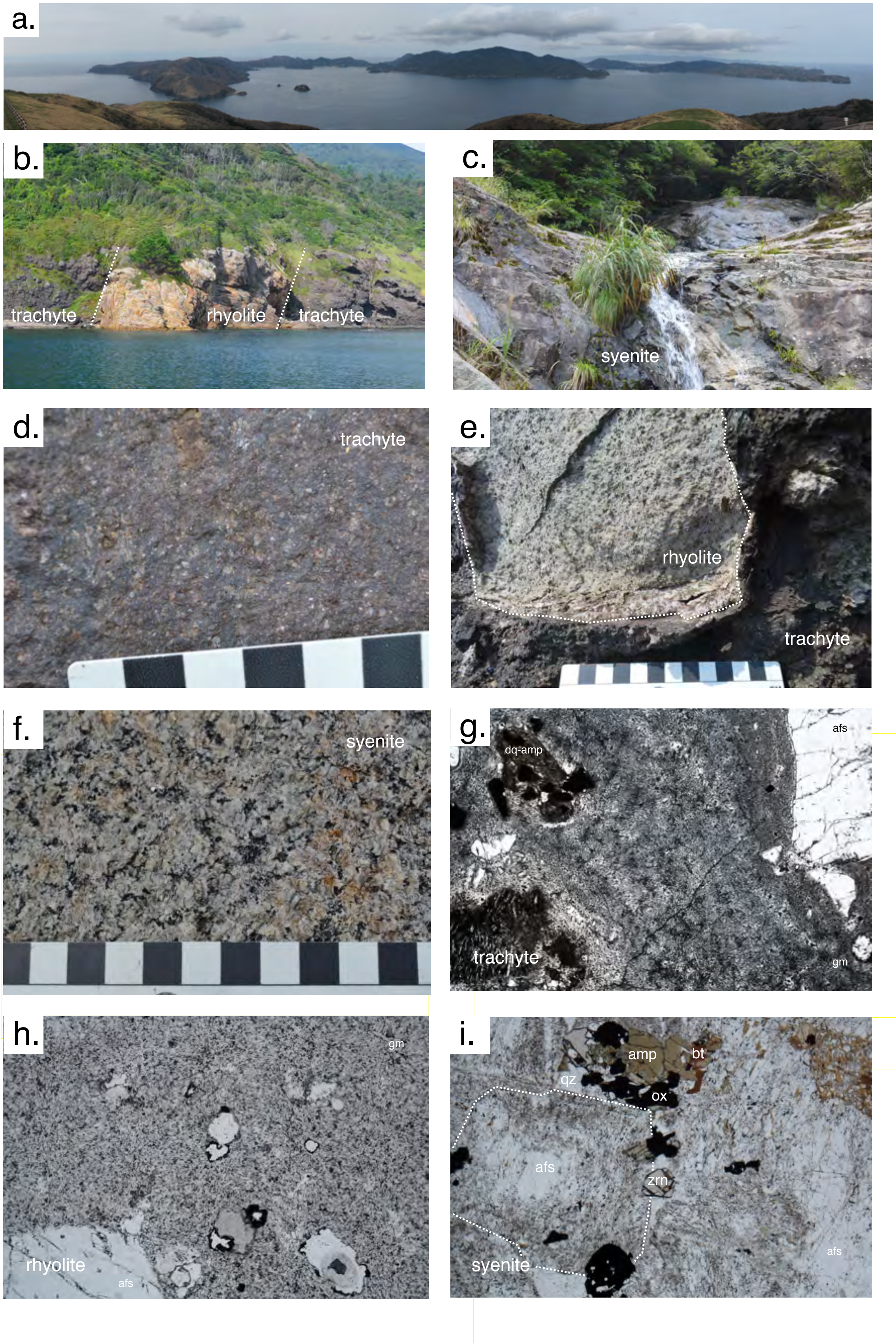
a.
b.
trachyte
rhyolite
trachyte
c.
syenite
d.
trachyte
e.
rhyolite
trachyte
f.
syenite
g.
dq-amp
afs
trachyte
gm
h.
gm
rhyolite
afs
i.
amp
bt
qz
ox
afs
zrn
syenite
afs

Fig. 3

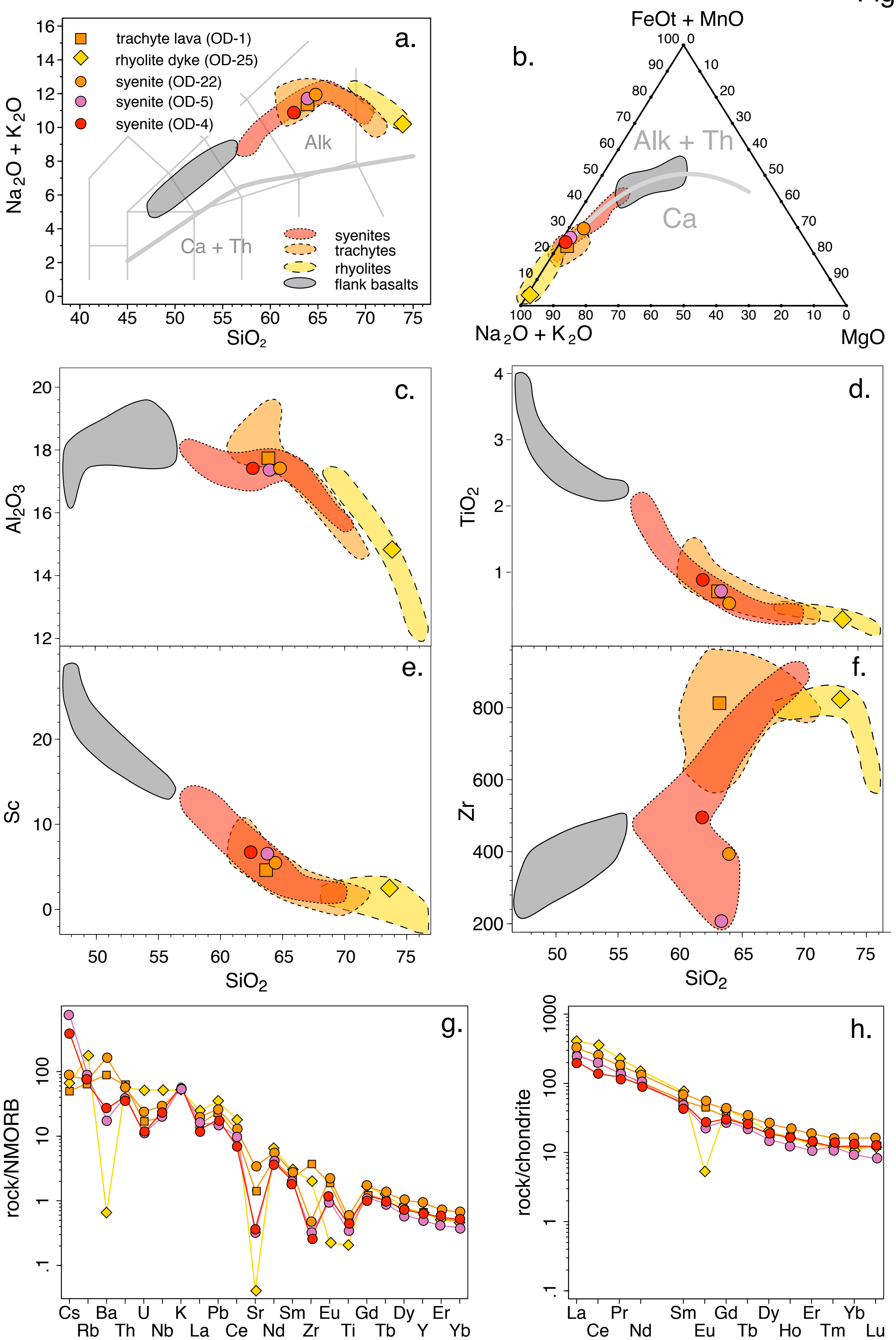
a.
trachyte lava (OD-1)
rhyolite dyke (OD-25)
syenite (OD-22)
syenite (OD-5)
syenite (OD-4)
Alk
Ca + Th
syenites
trachytes
rhyolites
flank basalts
Na2O + K2O
SiO2
b.
FeOt + MnO
Alk + Th
Ca
Na2O + K2O
MgO
c.
Al2O3
d.
TiO2
e.
Sc
f.
Zr
g.
rock/NMORB
Cs Rb Ba Th U Nb K La Pb Ce Sr Nd Sm Zr Eu Ti Gd Tb Dy Y Er Yb
h.
rock/chondrite
La Ce Pr Nd Sm Eu Gd Tb Dy Ho Er Tm Yb Lu

This is the peer-reviewed, final accepted version for American Mineralogist, published by the Mineralogical Society of America.
The published version is subject to change. Cite as Authors (Year) Title. American Mineralogist, in press.
DOI: https://doi.org/10.2138/am-2021-7861. http://www.minsocam.org/

Fig. 4

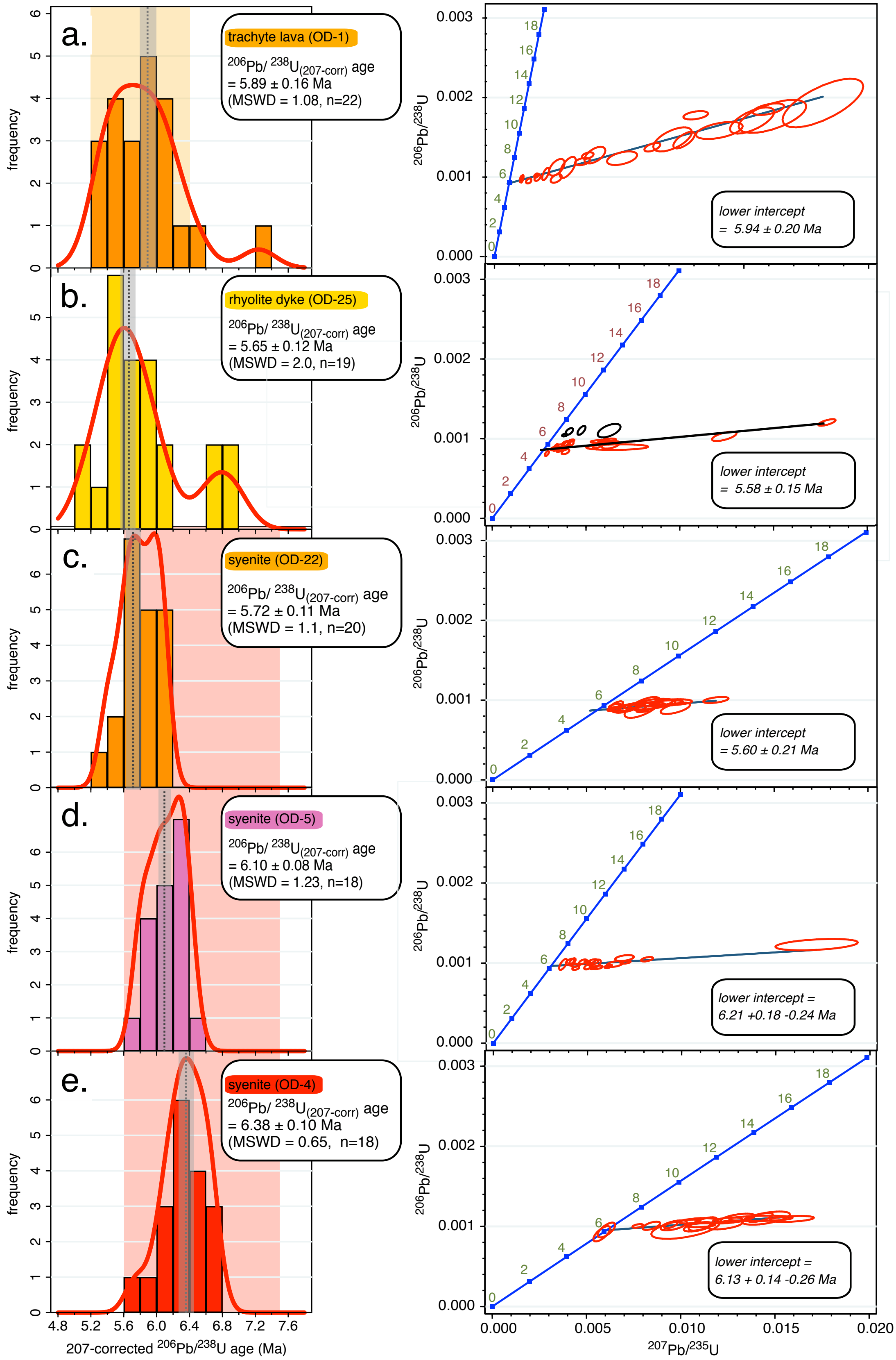

Fig. 5

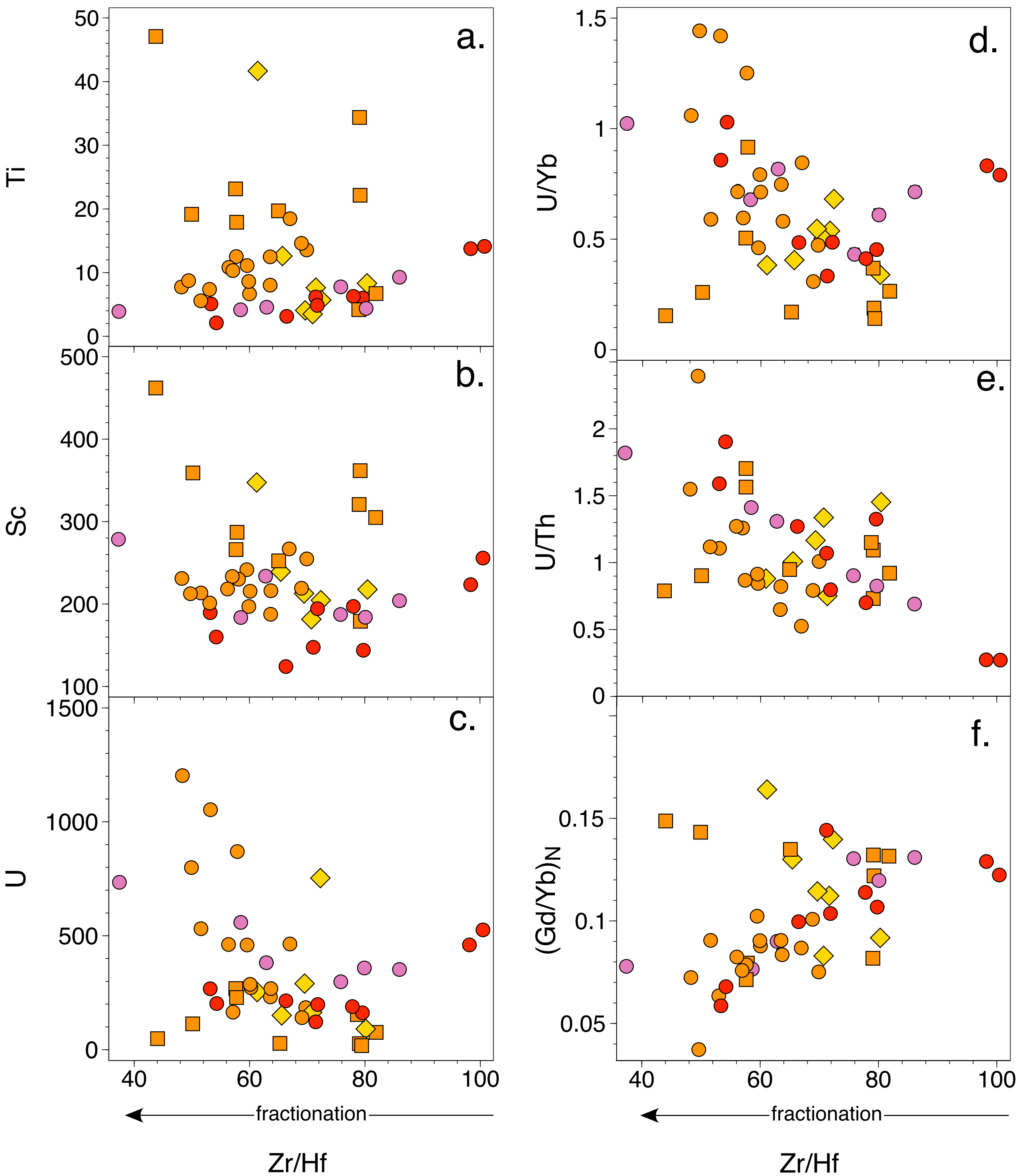
a.
b.
c.
d.
e.
f.
Ti
Sc
U
U/Yb
U/Th
(Gd/Yb)N
fractionation
fractionation
Zr/Hf
Zr/Hf

DOI: https://doi.org/10.2138/am-2021-7861. http://www.minsocam.org/

Fig. 6

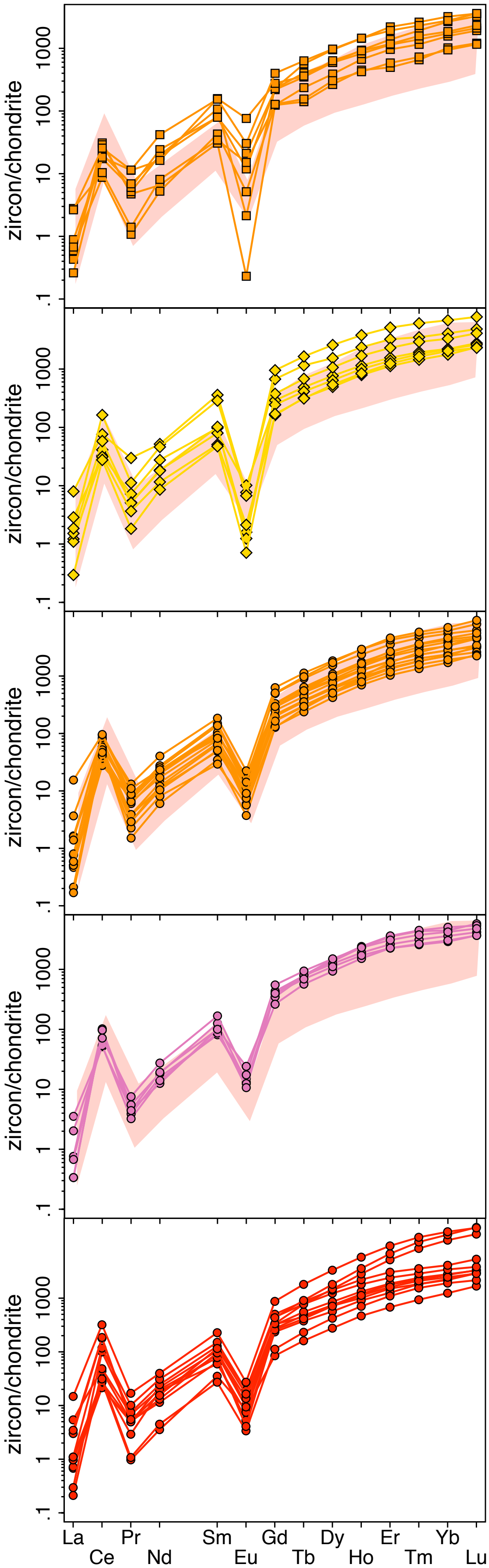

DOI: https://doi.org/10.2138/am-2021-7861. http://www.minsocam.org/

Fig. 7

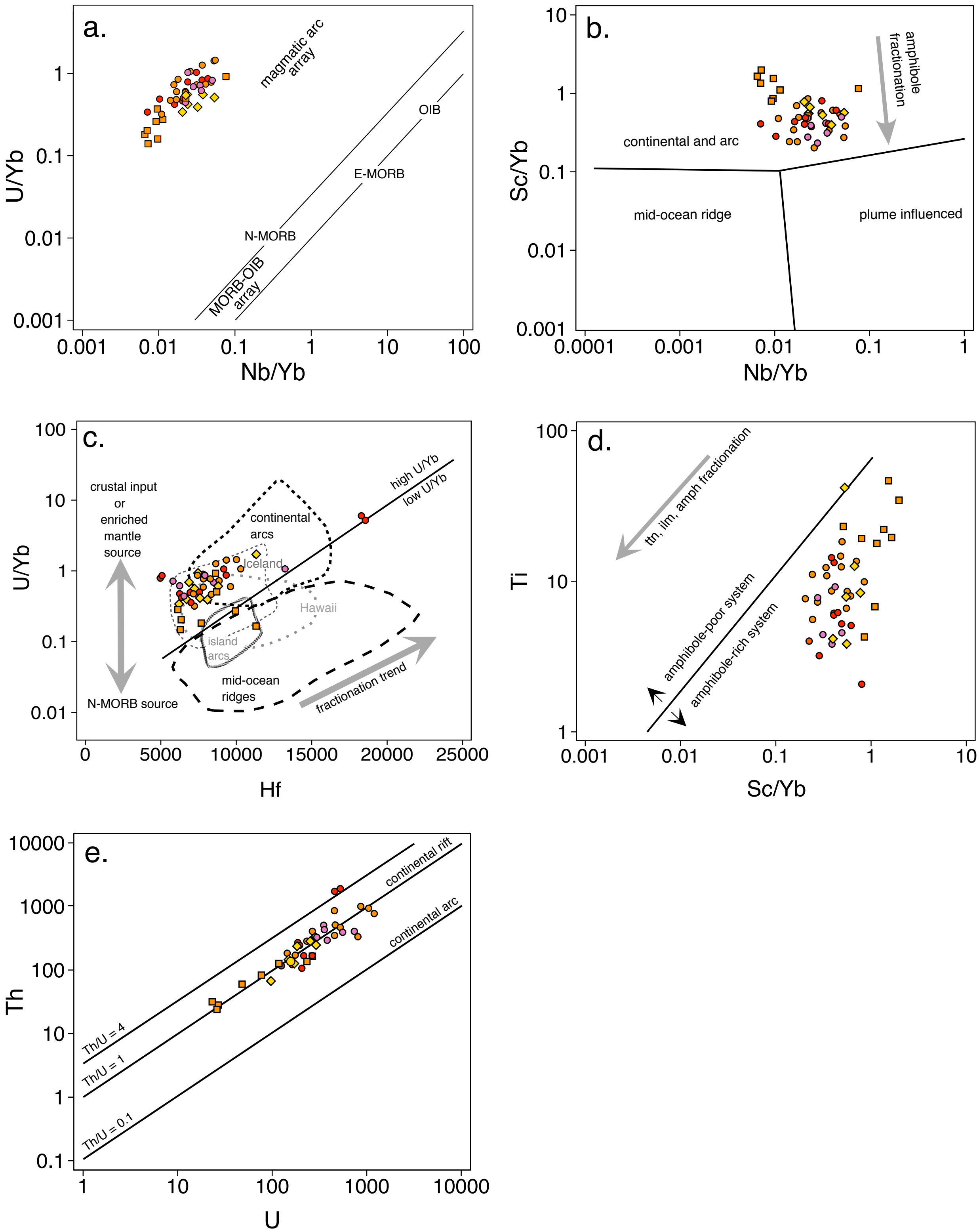

Fig. 8

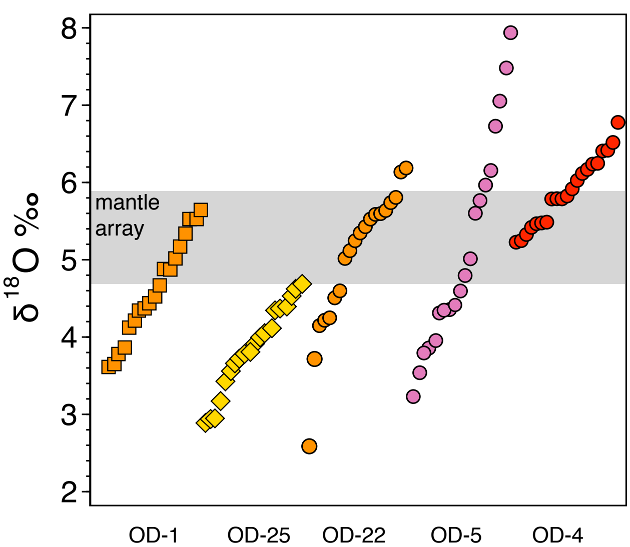

Fig. 9

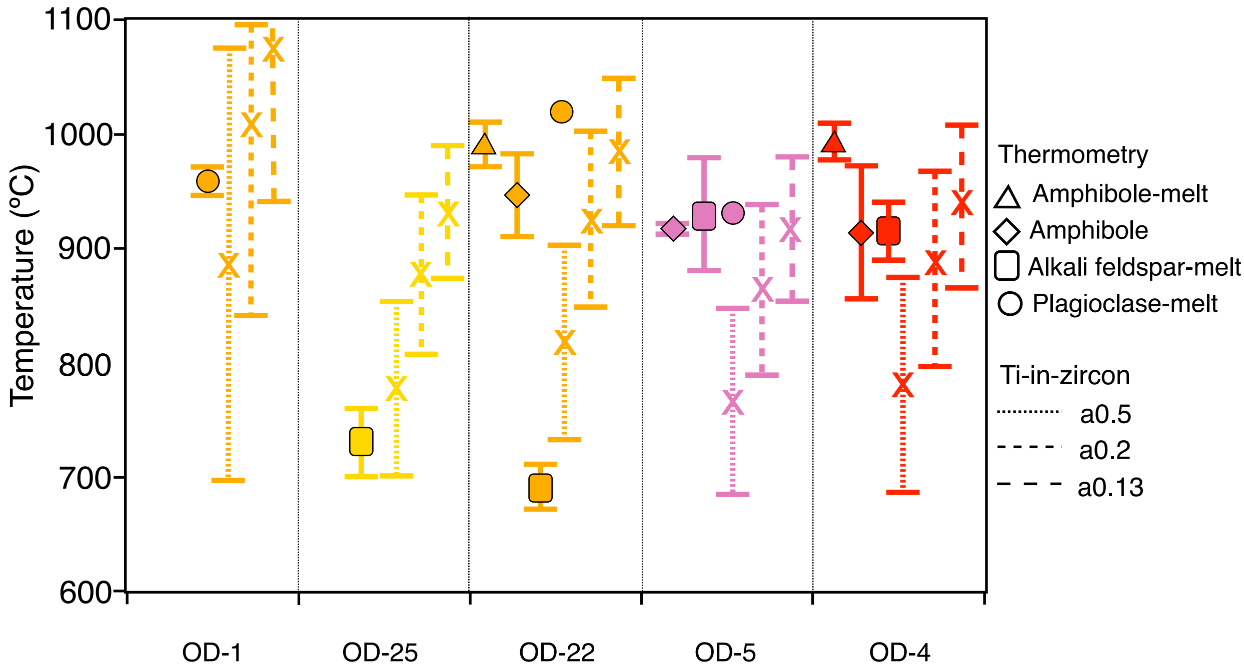
1100
1000
900
800
700
600
Temperature (ºC)
OD-1
OD-25
OD-22
OD-5
OD-4
Thermometry
Amphibole-melt
Amphibole
Alkali feldspar-melt
Plagioclase-melt
Ti-in-zircon
a0.5
a0.2
a0.13

Fig. 10

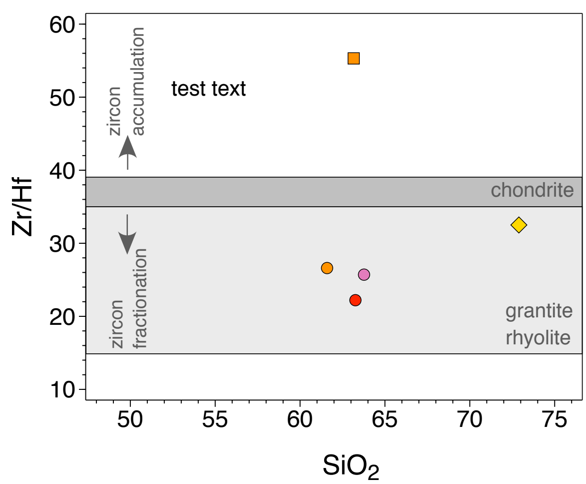
Zr/Hf
SiO2
zircon accumulation
test text
chondrite
zircon fractionation
grantite
rhyolite
60
50
40
30
20
10
50
55
60
65
70
75

This is the peer-reviewed, final accepted version for American Mineralogist, published by the Mineralogical Society of America.
The published version is subject to change. Cite as Authors (Year) Title. American Mineralogist, in press.
DOI: https://doi.org/10.2138/am-2021-7861. http://www.minsocam.org/

Fig. 11

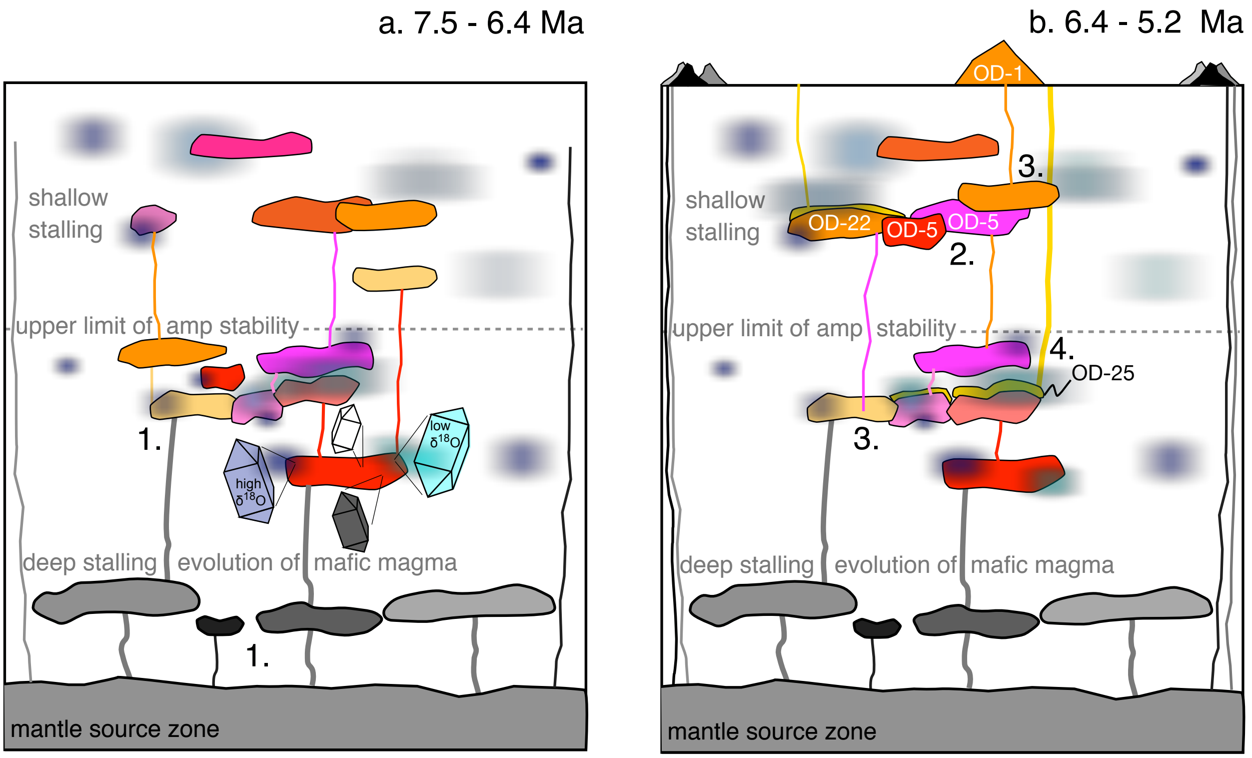

Plutonic and hypabyssal magmatism

Plutonic, hypabyssal and volcanic magmatism